A Study of Statistical Properties of Temporal Variations of X-ray Emission from NGC5548 in ROSAT PSPC Observations

Ludwik Liszka
Swedish Institute of Space Physics
Sörfors 634
S-905 88 Umeå
Sweden

Introduction

In the present report a technique to study long-term temporal variations of the X-ray emission from NGC5548 using ROSAT PSPC data is suggested. The capacity of the ROSAT PSPC instrument is described in The ROSAT Users´ Handbook.
The ROSAT satellite was primarily designed to study the spatial structure of X-ray sources. The temporal structure of the X-ray photon events will be influenced by the temporal variations of the source, the spacecraft wobble and the photon counting process in the instrument. Since the first and last process are Poisson processes, the resulting series of photon events will be a compound Poisson process modulated by the spacecraft wobble. In addition to that, if the source appears to have the extended X-ray emission (Morse, Wilson, Elvis and Weaver, 1995), the temporal variability of the source may be seriously obscured. In the present report, a possible statistical method to study temporal variations is shown. A list of analyzed ROSAT files is shown in Appendix 1.

Spatial properties of the X-ray emission from NGC5548 at low and high energies

The source NGC5548 shows a large content of low energy (<0.5 keV) photons forming a low energy peak in the energy spectrum (see Fig. 1)
It may be shown that photons in these two parts of the spectrum have different spatial and temporal behavior. The low energy peak (PI < 52 or energy < 0.5 keV) may correspond to the extended X-ray emission (Morse, Wilson, Elvis and Weaver, 1995). Another possibility is that the wide image at low energies is an instrumental effect, similar to that described for the High Resolution Imager (HRI) in ROSAT Users´ Handbook (pp. 90 - 102) as “halo”.
Examples of X-ray images for low and high energies, where photons were plotted as a function of sky coordinates, are shown in Fig. 2.
A photographic image of NGC5548 obtained from the Digitized Sky Survey is shown in Fig. 3.

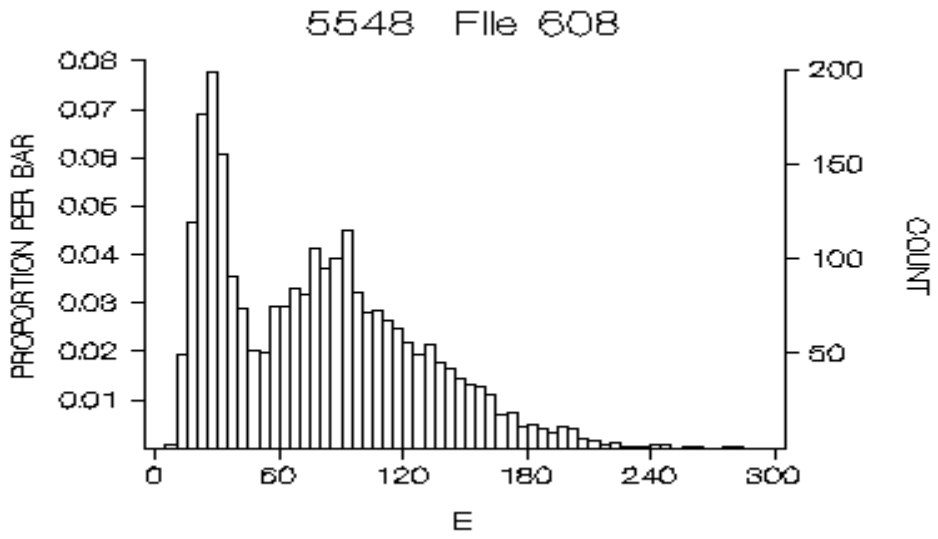

Fig. 1. A typical distribution of photon energy (channel number PI).

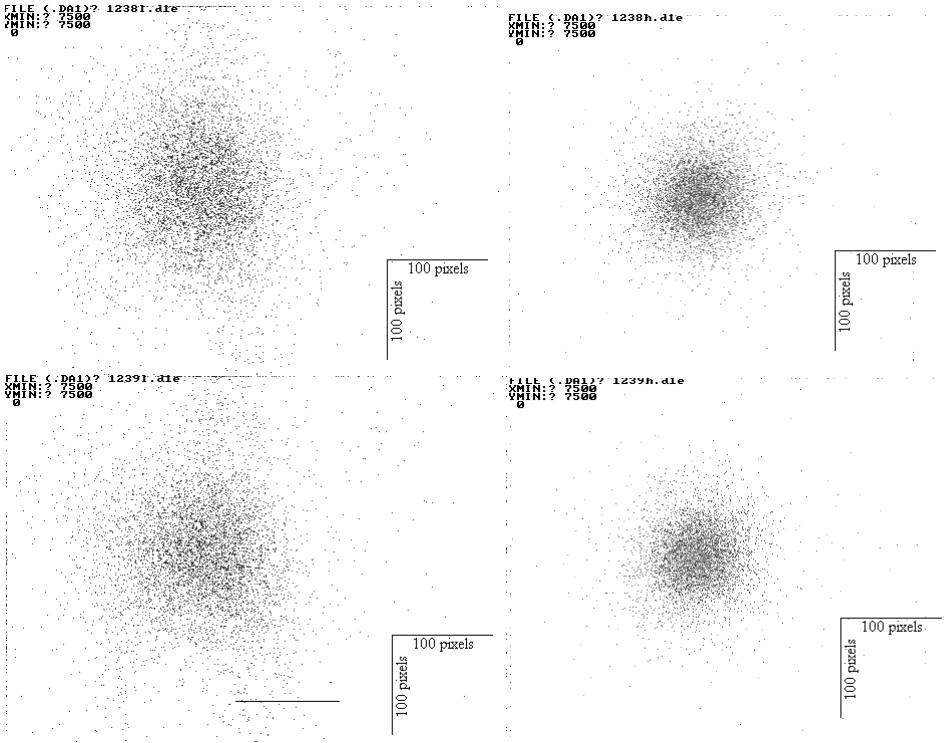

Fig. 2. Examples of X-ray images for low (left diagrams) and high (right diagrams) energies showing sky coordinates of single photons. 1 pixel corresponds to approximately 0.5". The R. A. is increasing towards the left and δ is increasing downwards

It is interesting to study the temporal structure of the low and high-energy images. For that purpose the history of photon events has been divided into 1-minute intervals and the spatial coordinates into 20 x 20 pixels bins, in total 12 x 12 bins. The center of the investigated area is located at X- and Y-pixels equal to 7698 and 7654. Although the resolution of PSPC is only 1 minute of arc, an attempt has been made to search for smaller structures in the image.

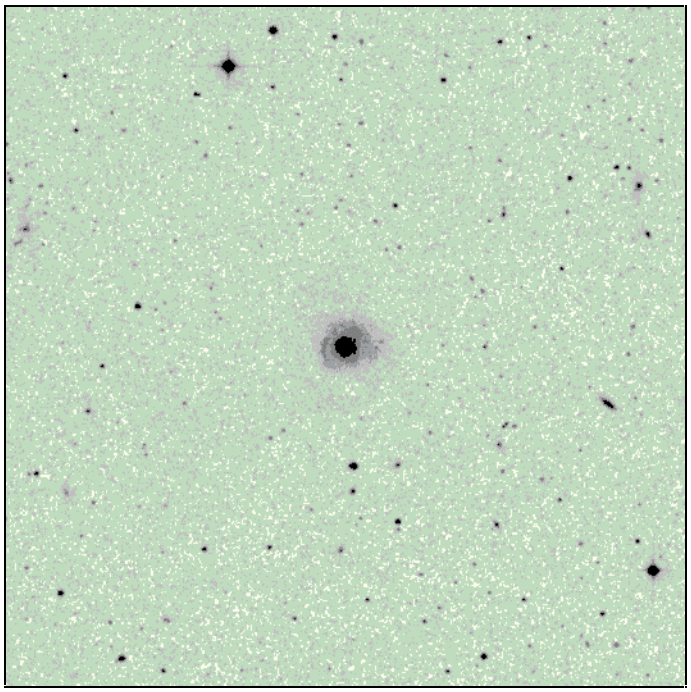

Fig. 3. A photographic image of NGC5548 obtained from the Digitized Sky Survey. The R.A. is increasing towards left and δ is increasing upwards.

For that purpose both averages and variances in individual bins were studied for all 22 files containing enough data. Isoplots of the average energy in each bin, expressed by the average energy channel, both for low and high energies, were constructed for all files listed in Appendix 1. Results are shown in Appendix 2 and 3. The isoplots may be compared with the photographic image shown in Fig. 4, which is an enlarged part of Fig. 3, with approximately the same scale as the isoplots.

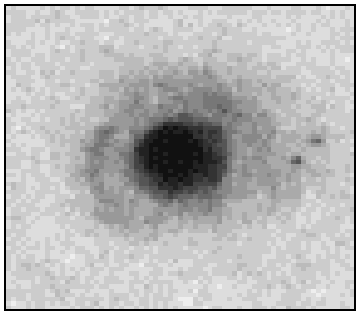

Fig. 4. An enlarged part of Fig. 3. showing NGC5548 with approximately the same scale as the scale of isoplots in Appendix 2 - 5.

It may be seen, especially in Appendix 2 (low energies), that some structures are repeated in the same bins during consecutive files (days). That may be an indication that those structures are real, and not produced accidentally by photon fluctuations.

Another method to study the structure of the image is to calculate the variance of energy in each individual bin of all 22 files. For each file an isoplot of energy variance may be constructed in the same way as for the average energy. The results of the study are shown in Appendix 4 (low energy) and in Appendix 5 (high energy). An interesting property of the variance isoplots may be observed. There seems be a ring of high variance of energy with a diameter of about 160 arc seconds at low energies and with a diameter of about 120 arc seconds at high energies. The structure of the ring has also a time constant comparable with the time interval between files. The average isoplots of all 22 files are shown in Fig 5 below.

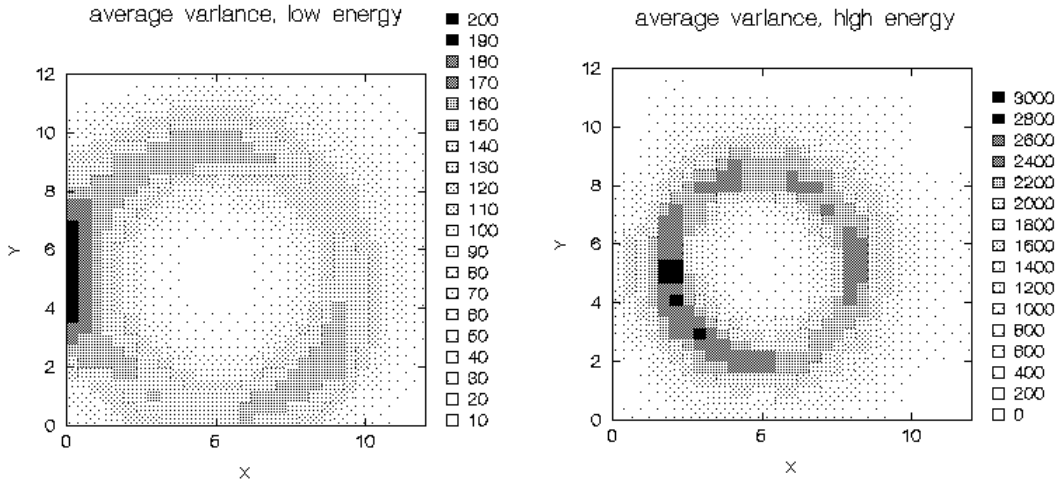

Fig. 5. Average isoplots of the energy variance for all 22 files and the low energy part of the spectrum (left) together with the isoplots for the high-energy part of the spectrum (right).

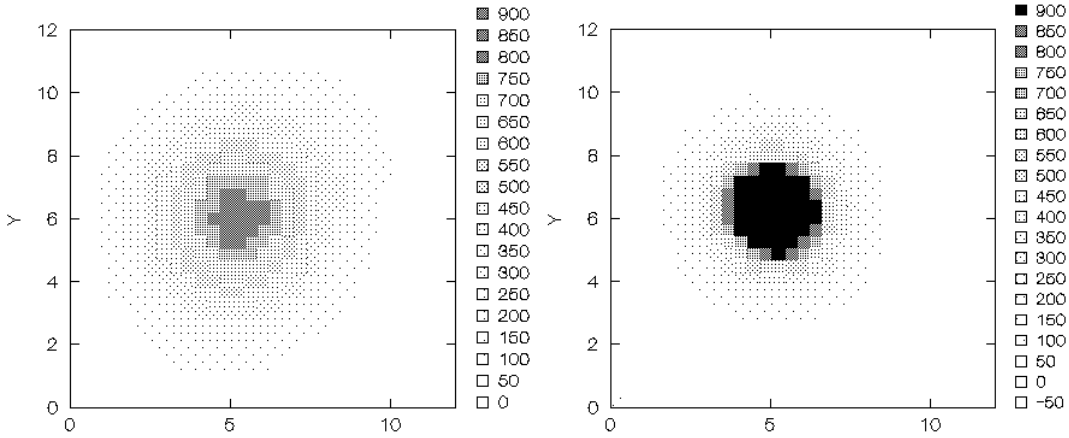

Fig. 6. Isoplots of photon counts for file 1271, for low (left) and high (right) energy part of the spectrum.

Number of photon counts per bin increases dramatically within the core of the image. It may be seen in Fig. 6 showing isoplots of photon counts for a typical file. In spite of that fact, the variance of energy is stable and very low within the core; only a small fraction of that for the ring.

An attempt has been done to study the nature of variance. Of all 12 x 12 bins only 10 x 10 bins (X-bins # 1 - 10 and Y-bins # 2 - 11) have been selected to perform the causal analysis (Glymour et al (1987) and Spirtes et al (1993a)) of the energy data.

For all selected 100 spatial bins all temporal 1-minute bins have been collected forming thus a matrix of dimensions: 100 x number of 1-minute bins. Such a matrix was formed for both low energy (PI<52) and high energy (PI>52) photons. The low energy matrix consisted of 685 1-minute intervals and the high-energy matrix of 702 1-minute intervals. The causal analysis of the data was then performed using the TETRAD II software. The aim of the analysis was to find linear dependencies between the bins in the image and to find the direction of the dependencies. The TETRAD II software finds these dependencies and is able to establish if some image bins are the cause of some other image bins. If the photons in the image are originated in different part of the source, the causal relations between energies in the different parts of the image are very unlikely due to the immense size of the source comparing with the short time scale of the observations. However, if the fluctuations of the photon flux are due to instrumental effects, e. g. due to the wobble of the spacecraft, it may be expected, that the image bins will be causally related across the image. In particular, it may be expected that the bins of the ring should be strongly related.
Results of the causal analysis for low and high energies are shown in Fig. 7. The analysis has been performed at the significance level of 0.01.

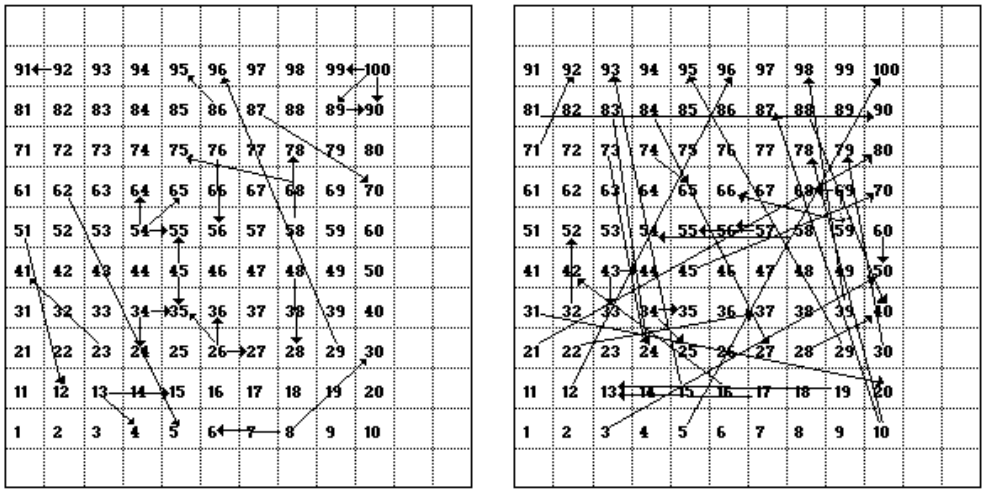

Fig. 7. Results of TETRAD analysis for the average low (left) and high (right) energy image. Arrows indicate the presence of linear relations between the image bins and the directions of the relations (causality). The area of the graph corresponds to the area of each isoplot of Figs. 5 and 6.

An examination of the above graphs indicates that in the high-energy image there are significant causal relations across the ring surrounding the core of the image. That is an indication that the variance of photon energy in the ring if of the instrumental origin. A different situation is observed for the low energy image. Most of causal relations (directed edges) observed here are between adjacent or close bins in the image. These edges may be due to a limited resolution of the detector showing the real energy leakage between the close bins. There are only two directed edges ranging across the ring. A straightforward conclusion of that observation must be that in the low energy part of the X-ray spectrum there may be significant structures in the image. It may be due to the fact that the source has apparently larger angular dimensions at low energy and that the resolving power of the instrument may be just enough to detect these structures.

Another conclusion of the above analysis is that the core of the image, showing high counting rates of photons, low variance of energy and no causal relations which may indicate instrumental effects, should be most suitable for the search for the true temporal variations in the source. In the next section the central part of the core will be used to search for temporal variations.

Temporal variations of the X-ray flux

Analytical procedure

The central part of the image core is divided into four equal areas according to the following procedure:
- An approximate center of the image is determined manually.
- From the approximate center of the image 4 squares, 15 x 15 pixels large, with one common corner are constructed (see Fig. 8).
- All photons (at all energies) are then counted within the 4 areas.
- If the total number of photons is found to differ between the 4 areas, the location of the center is adjusted until the equality is achieved.

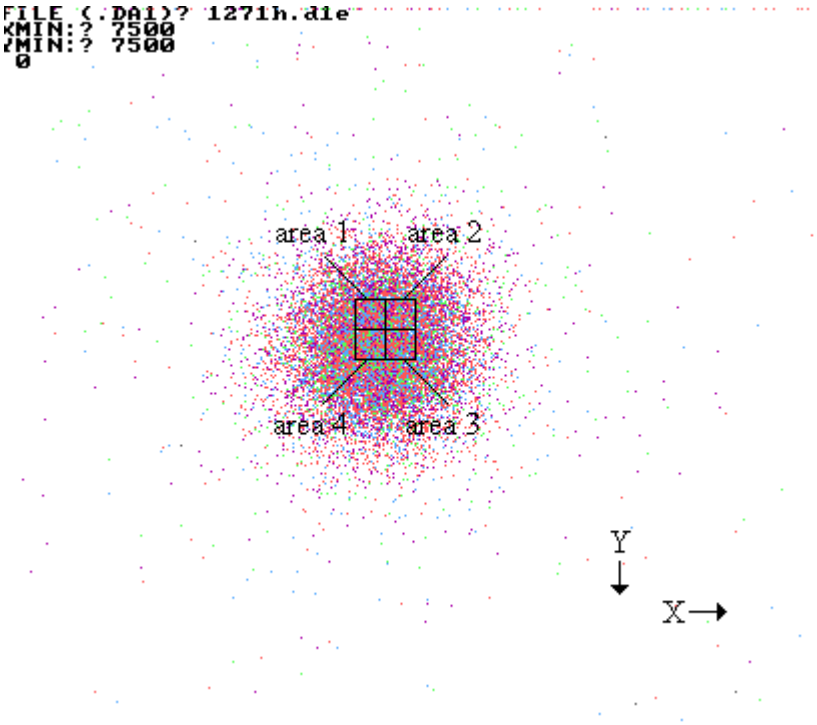

Fig. 8. Positions of the 4 areas on the photon plot. Origo in the upper left corner.

It has been found that, in spite of the above-mentioned procedure, the photon counts may differ between the 4 areas after photons were divided into low (PI < 52) and high (PI > 52) energy populations.
It may be expected that an externally originated Poisson process will appear synchronously in the 4 areas of the image. Likewise will the photon count variation due to the spacecraft wobble be related in the 4 areas according to the geometry of the

wobble. The Poisson process due to photon counting in the detector will be entirely uncorrelated between the 4 areas.

Variables studied:
There are four variables studied:
- T, average time interval between 32 consecutive photons
- Var(T), variance of time intervals between 32 consecutive photons
- E, average energy channel for 32 consecutive photons
- Var(E), variance of the energy channels for 32 consecutive photons.

The above variables are determined both for low and high-energy part of the photon population.

The spacecraft wobble and the aspect solution
The spacecraft wobble is, according to the ROSAT User's Handbook, parallel to one of the PSPC support ribs. The real wobble is much more complicated. Due to a small phase difference between X- and Y-component of the wobble, the aspect axis of the spacecraft moves along a narrow ellipse, sometimes slightly irregular. An example of the trajectory of the aspect axis in the XY-plane during a single wobble period is shown in Fig. 9.

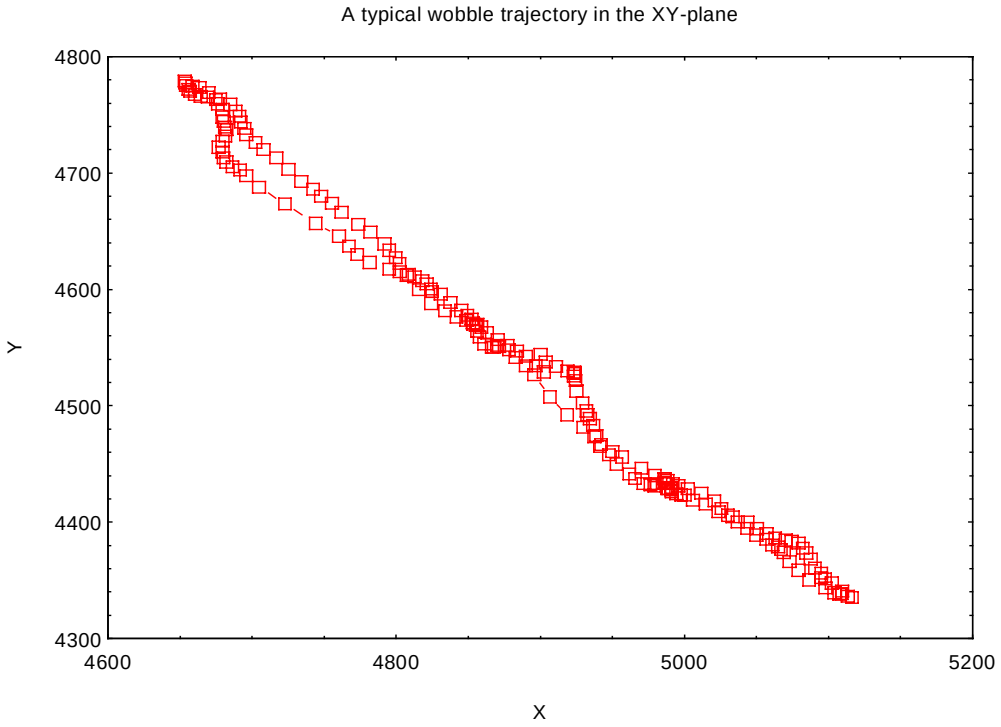

Fig. 9. An example of the trajectory of the aspect axis in the XY-plane during a single wobble period

Studying the temporal variations of the photon flux it is of importance to determine the relation between the photon counts and the phase of the satellite wobble. It has been found that the aspect files, containing the information about the both components of the wobble, are not always available for all FITS-files of interest. In order to compare the observed variations of the above defined variables with the wobble phase, without using the aspect files, the following procedure has been used:

1. A small portion of the image, 30 x 30 pixels large, centered around the center of the image, where the number of photon events is largest, is selected.
2. For that area the detector coordinates are plotted as a function of time.
3. By smoothing the curve, the aspect variations, practically identical with those contained in aspect files, are obtained.
4. The DC-level of the curve is determined as a function of time.
5. The ascending crossings of the curve with the DC-level are calculated and used as points of 0-phase.
6. The phase angle φ_i is calculated for each individual photon event i, assuming that the phase is changing linearly between two consecutive phase zeros.
7. For each 32 consecutive photon events the average of sin φ_i is calculated to be used for comparison with the studied variables, being also 32 point averages.

If photon events would be uniformly distributed throughout the entire wobble cycle, the average value of sin φ_i would be equal zero. However, most frequently, the average value of sin φ_i differs from zero. Two examples of average values of sin φ_i for all 4 areas are shown in Fig. 10 as a function of time. The upper diagram shows a small effect of the wobble, the lower diagram shows a strong effect of the wobble phase on the occurrence of photon events.

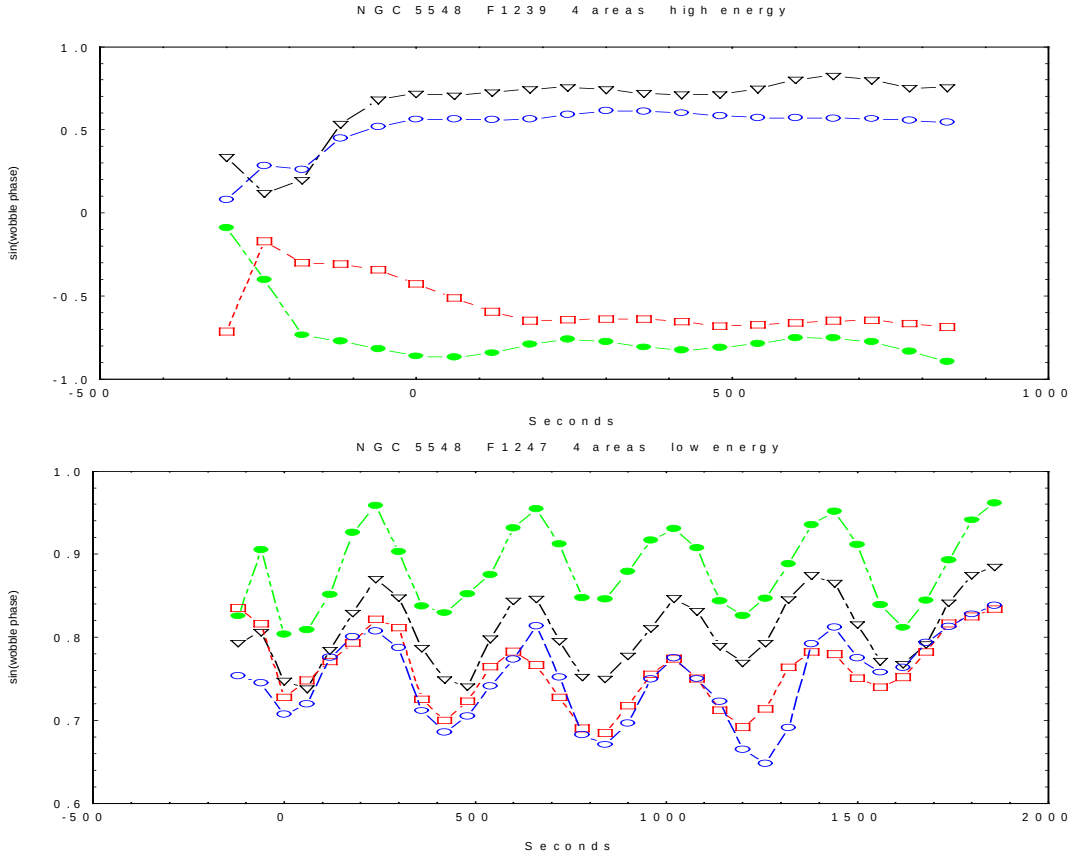

Fig. 10. Two examples of average values of sin φ_i for all 4 areas shown as a function of time

Results

Are photon events a Poisson process?

The first question, which must be raised when studying the time series of photon events, is whether the observed process is really a Poisson process. For a Poisson process the variable T and Var(T) must be equal to the process parameter λ. It has been found that for the photon data that is almost never the case. An example of variations of T and Var(T) during a period of observations is shown in Fig. 11.

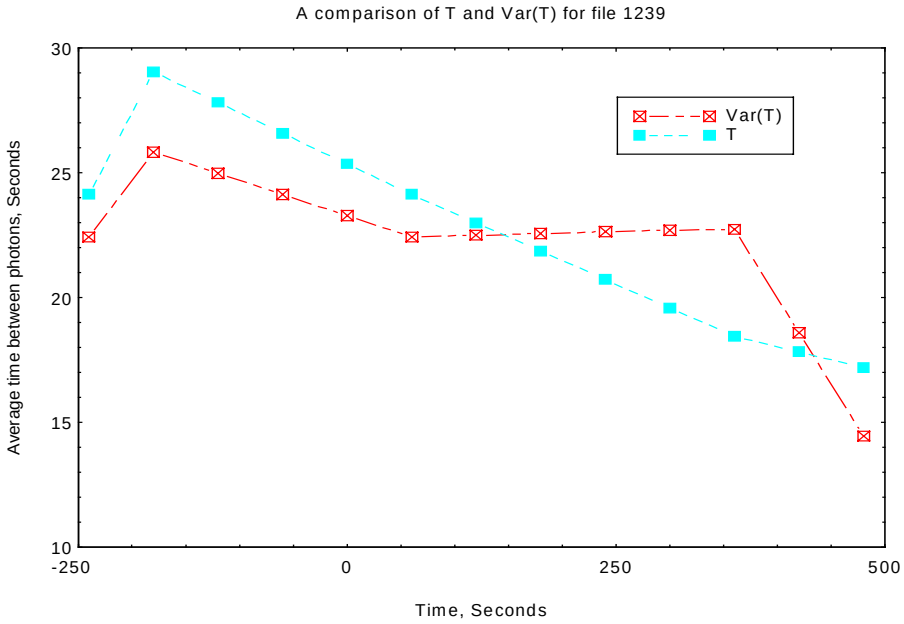

Fig. 11. An example of variations of T and Var(T) during a period of observations, file # 1239.

The statistical relation between Var(T) and T has been studied for the actual data. Assuming a linear relation between the variables of the type:

$$\mathrm{Var}(T) = b\,T + a$$

the linear coefficient b may be calculated for all files (data sets). The value of b both for low and high-energy photons is given in Fig. 12 as a function of time (days after December 1, 1992).

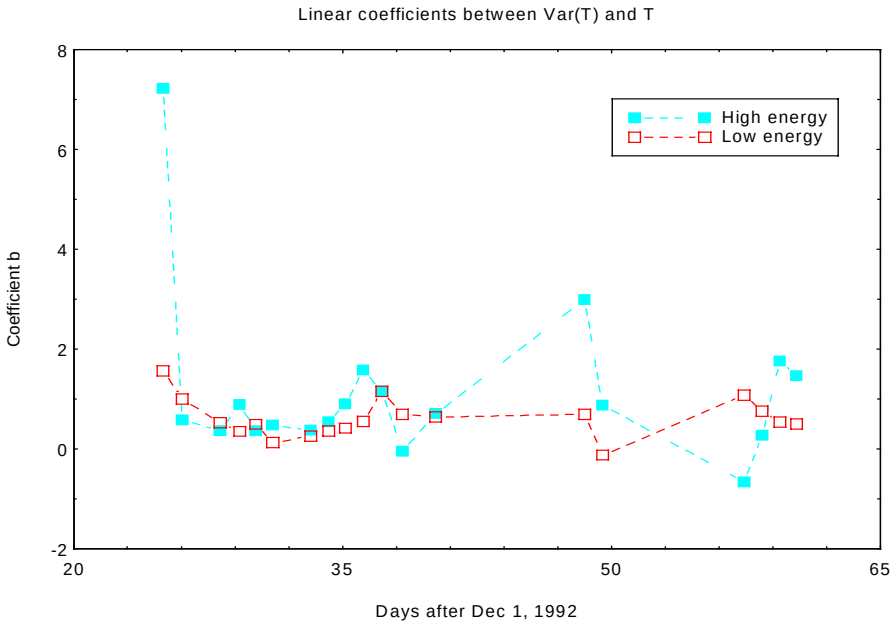

Fig. 12. Values of the linear coefficient b between Var(T) and T both for low and high-energy photons as a function of time (days after December 1, 1992).

If the time series of photon events would be a Poisson process T and Var(T) would be equal, i. e. a = 0 and b = 1. b>1 corresponds to the situation where Var(T) > T.

Temporal variations

The variables: T, Var(T), E and Var(E) determined for all four areas of the image core will be used to search for true temporal variations. It is assumed that the part of the image, used for the present analysis is, in the whole image, less influenced by the wobble. What is left of that influence, will differ in phase in the four areas. A vector of 16 variables defined as follows:

$$T_i, (Var(T))_i, E_i, (Var(E))_i \quad \text{where} \quad i=1,...4 \qquad (*)$$

may be used to search for true temporal variations.

An example of temporal variations of all variables for all four areas are shown in Figs. 13 (low energy photons) and 14 (high-energy photons) for one period of observations (file # 1273).

Following conclusions may be drawn from the diagrams:

- There are large differences between counts and energies and their variances in all 4 areas. Differences between the photon counts are largest for low energy photons. The phenomenon may be of the same nature as the image asymmetry described for the High Resolution Imager (HRI) in ROSAT Users´ Handbook (pp. 90 - 102).
- The wobble component (400 seconds) is clearly seen in some areas in high-energy data (see Fig. 15), and is still possible to trace in the low energy data.

It must be remembered that the variables forming the above vector cover different periods of time (are not read simultaneously). The variables are therefore corrected to a common time base (1-minute intervals) assuming linear variations between the adjacent values.

A matrix consisting of N 16-component vectors, where N is number of 1-minute intervals during one period of observations, is constructed for each period of observations, both for the low and high-energy populations of photons.

A joint matrix **B**, consisting of matrices from all 22 observing periods was constructed, one for each energy interval.

The next step of the analysis was to perform the principal component analysis (PCA) for each joint matrix. The results of PCA were:

- The vector of eigen values of the joint matrix, telling how much of the total variance in the matrix may be explained by the consecutive principal components.
- The matrix of component score coefficients **a**, a transformation matrix between the old system of 16 variables and the principal components (the new coordinate system).
- The matrix of component scores **S**, with one column for each principal component, being a projection of old 16 variables upon the new coordinate axis (directions of principal components).

Each principal component represents an independent mechanism controlling the variations of the 16-component vector, which instantaneous values are gathered in the matrix **B**.

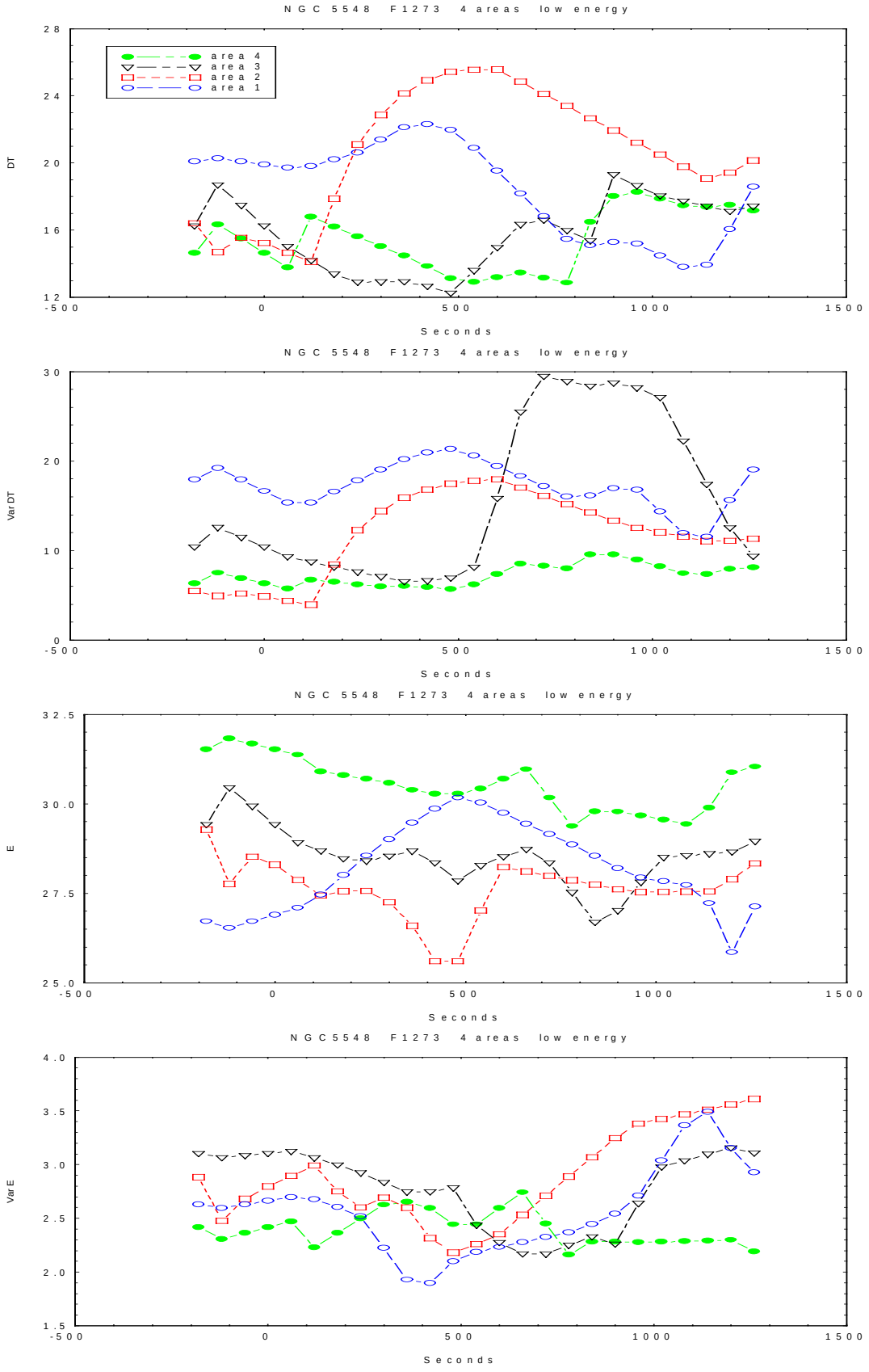

Fig. 13. An example of temporal variations of 32-photon averages of: time interval between photons (T), variance of T, average energy channel (E) and variance of E for all 4 areas in the image, low energy part of the spectrum (PI<52), file # 1273 of January 9, 1993.

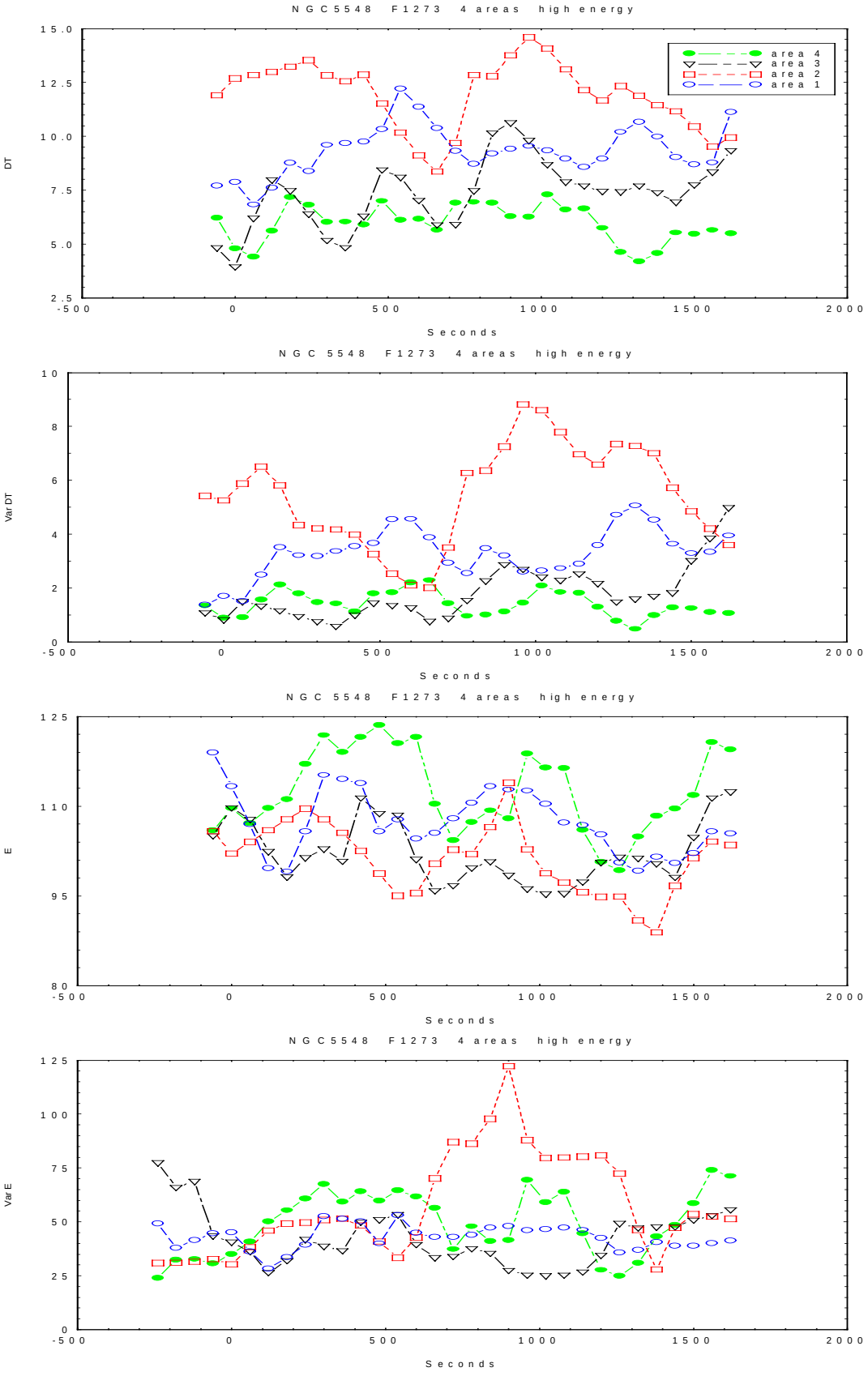

Fig. 14. An example of temporal variations of 32-photon averages of: time interval between photons (T), variance of T, average energy channel (E) and variance of E for all 4 areas in the image, high energy part of the spectrum (PI<52), file # 1273 of January 9, 1993.

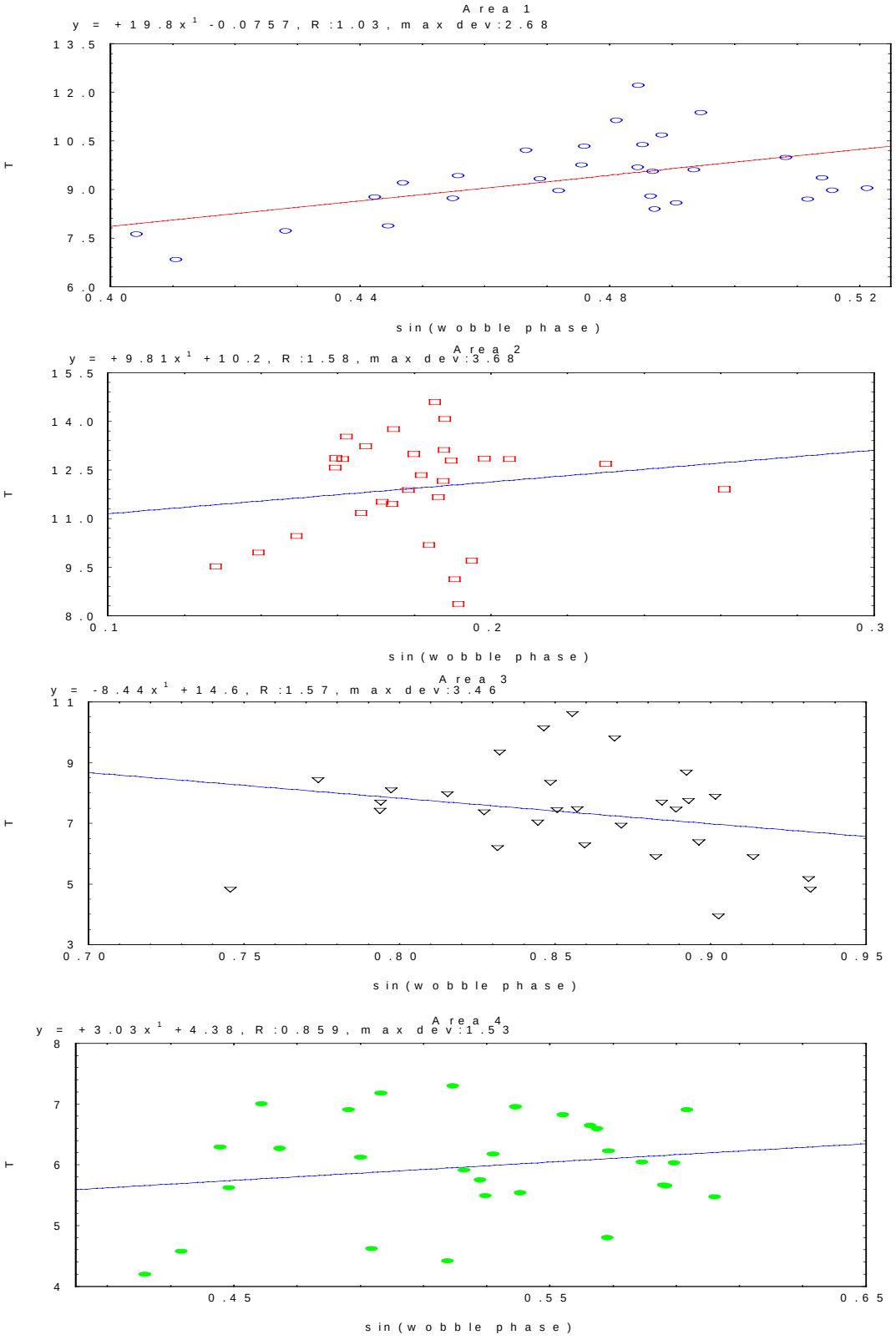

Fig. 15. The average time interval between 32 photons as a function of spacecraft wobble ($\sin \varphi_i$) for all 4 areas, high-energy photons.

If one wants to know what the variations of the 16-component vector would be with only one mechanism, corresponding to the principal component *l* active, it is possible

to mask all other columns in **S**, except of column *l* and to perform a calculation of a new matrix $\mathbf{B}_l$:

$$\mathbf{B}_l = \mathbf{S} \cdot \mathbf{a}^{-1}$$

The operation may be repeated for each interesting component *l*.
It is obvious that the component (or components) corresponding to true temporal variations of the photon flux, and thus the average time interval T, will vary synchronously in all four areas. The components generated by the spacecraft wobble will have the opposite phase in some areas, depending on the orientation of the wobble.
Similar calculations have been done for 8-component vector containing only T and Var(T) for all 4 areas. It has been found that results of such calculations are much easier to interpret, probably because the photon energy is almost uncorrelated with the photon flux. In the next section a summary of 8-component study is given.

Results of PCA

Principal component analysis made for all 22 observation periods simultaneously indicate that there are 2 significant principal components for the low energy data and 3 significant principal components for high energy data. The percentage of total variance explained by these principal components is shown below.

PC1	PC2	PC3
Low energy		
75.2%	10.1%	-
High energy		
54.5%	13.8%	12.8%

Examples of temporal variations of the average time interval between 32 photons, T, for all 4 areas and corresponding to the significant principal components, are shown in Figs. 16 and 17.
For low energy photons (Fig. 16) it may be seen that T values calculated for the most important principal component have the same sign in all four areas. That component is responsible for about 75% of total variance. The second principal component explains about 10% of the total variance. That component corresponds to variations of photon flux in areas 2 and 4, which are similar in shape, but with opposite signs. That component is most likely due to the spacecraft wobble.
For high-energy photons (Fig. 17) there are 3 significant principal components. The first one, which has the same sign in all four areas, corresponds to about 55% of total variance. Remaining two components, corresponding to about 26% of total variance are anti-correlated between different areas and are probably caused by the spacecraft wobble. 400-seconds variation is clearly seen in the 2nd (and even in the 3rd) component.
The T values calculated from the first principal component are most likely showing gross temporal variations of the photon flux, although there is still a trace of 400-seconds variation. That means that there must be a component of wobble influence which is synchronous in all 4 areas. The T values calculated from less significant principal components are much smaller than for the first principal component. However, it does not mean that these values correspond to higher photon fluxes than

those corresponding to the first principal component. These values should be rather considered as corresponding to **deviations** from the main component.

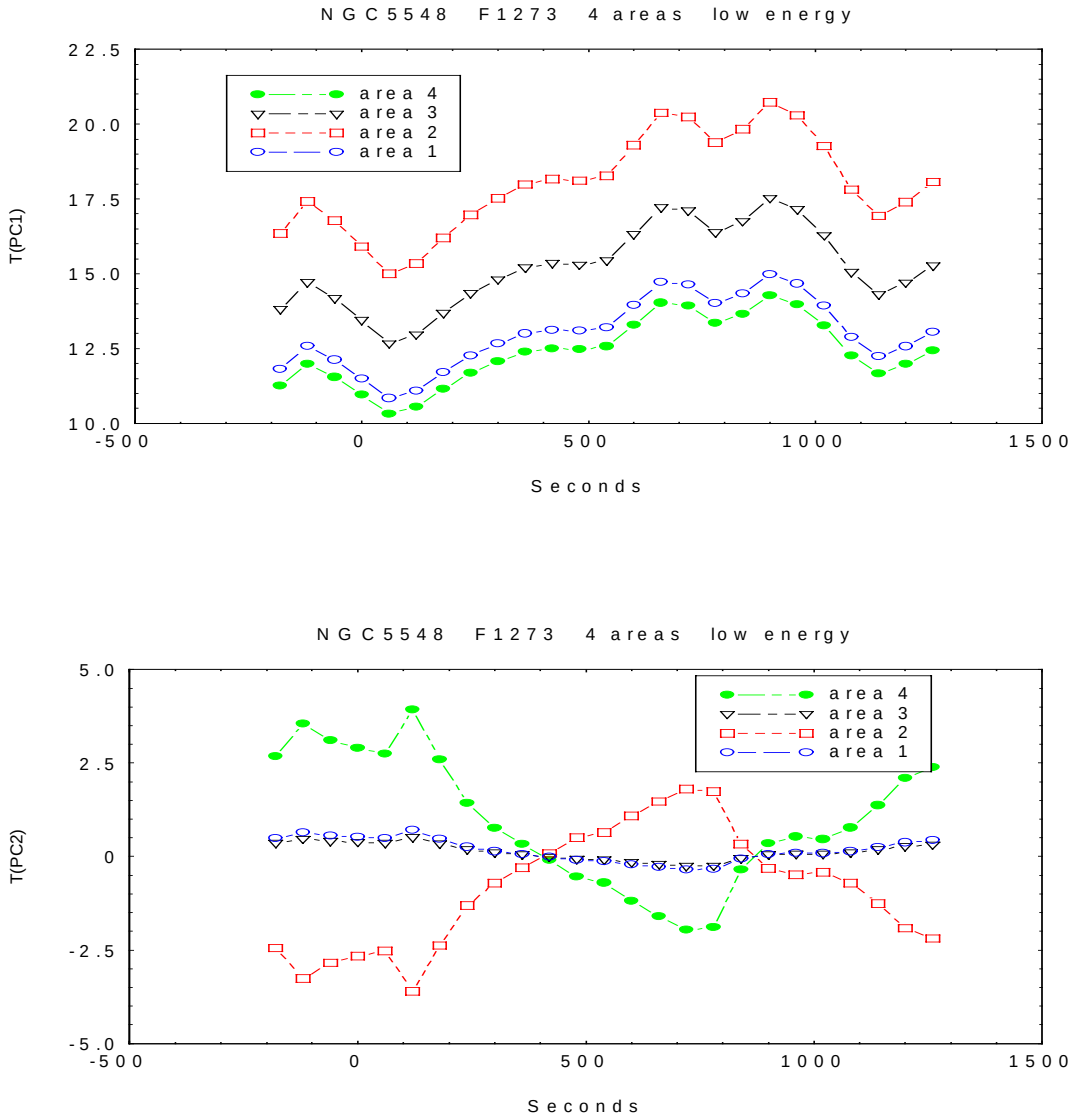

Fig. 16. An example of temporal variations of the average time interval between 32 photons, T, for all 4 areas and corresponding to the significant principal components. File # 1273, low energy.

It may be seen in Figs. 16 and 17 that the temporal variations of the main component are frequently faster at high energy than at low energy. In Fig. 17 there is, for PC1, in the middle of the graph, a rapid drop of the photon flux by almost a factor of 2. This kind of temporal variations is frequently observed for high-energy photons.

The average time intervals between photon events in individual areas may be used to calculate the average T for all 4 areas. That must be done averaging the corresponding photon fluxes rather than the time intervals. The results of the averaging have been plotted as the function of time of observation for low- (Fig. 18) and high-energy (Fig. 19) photons. It may be seen that the first component at low energy shows large temporal variations during the period of observations (December 24, 1992 - January 29, 1993). Variations of T due to the wobble are during that period less than +/- 2 sec for low energy and less than +/- 1 sec for high energy.

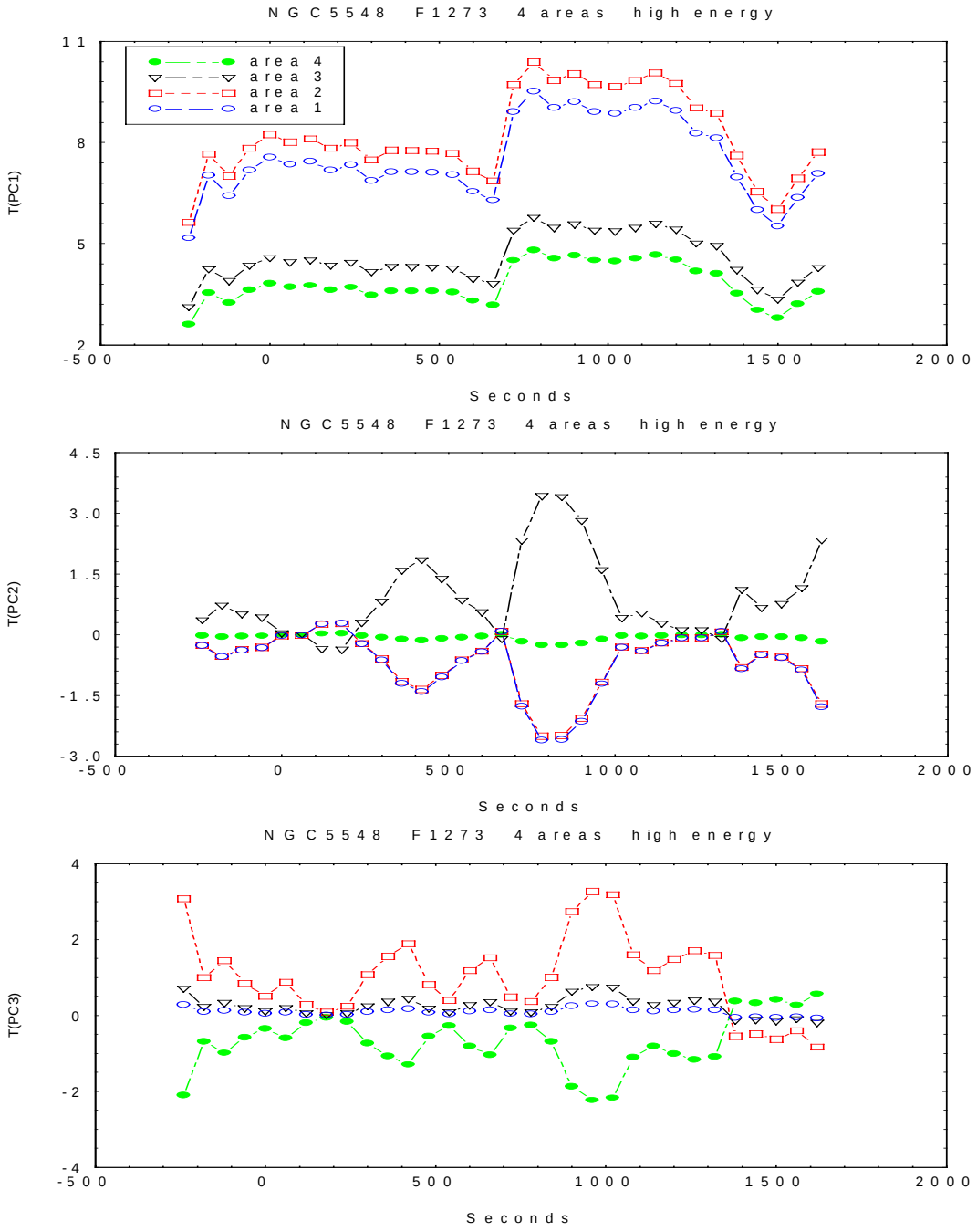

Fig. 17. An example of temporal variations of the average time interval between 32 photons, T, for all 4 areas and corresponding to the significant principal components. File # 1273, high energy.

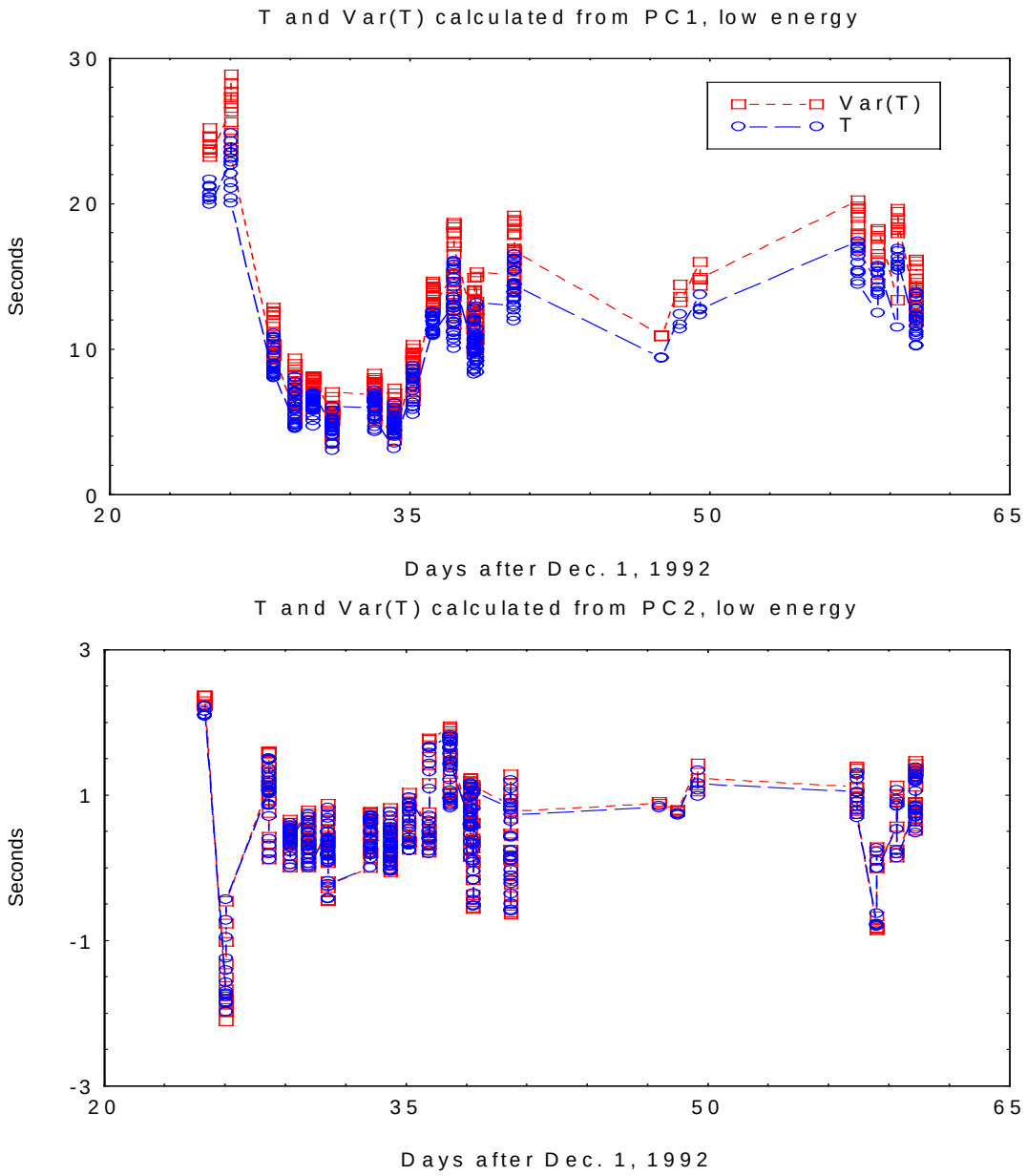

Fig. 18. Temporal variations of the average time interval between 32 photons, T, and Var(T) averaged over all 4 areas, corresponding to the significant principal components: PC1 and PC2. File # 1273, low energy.

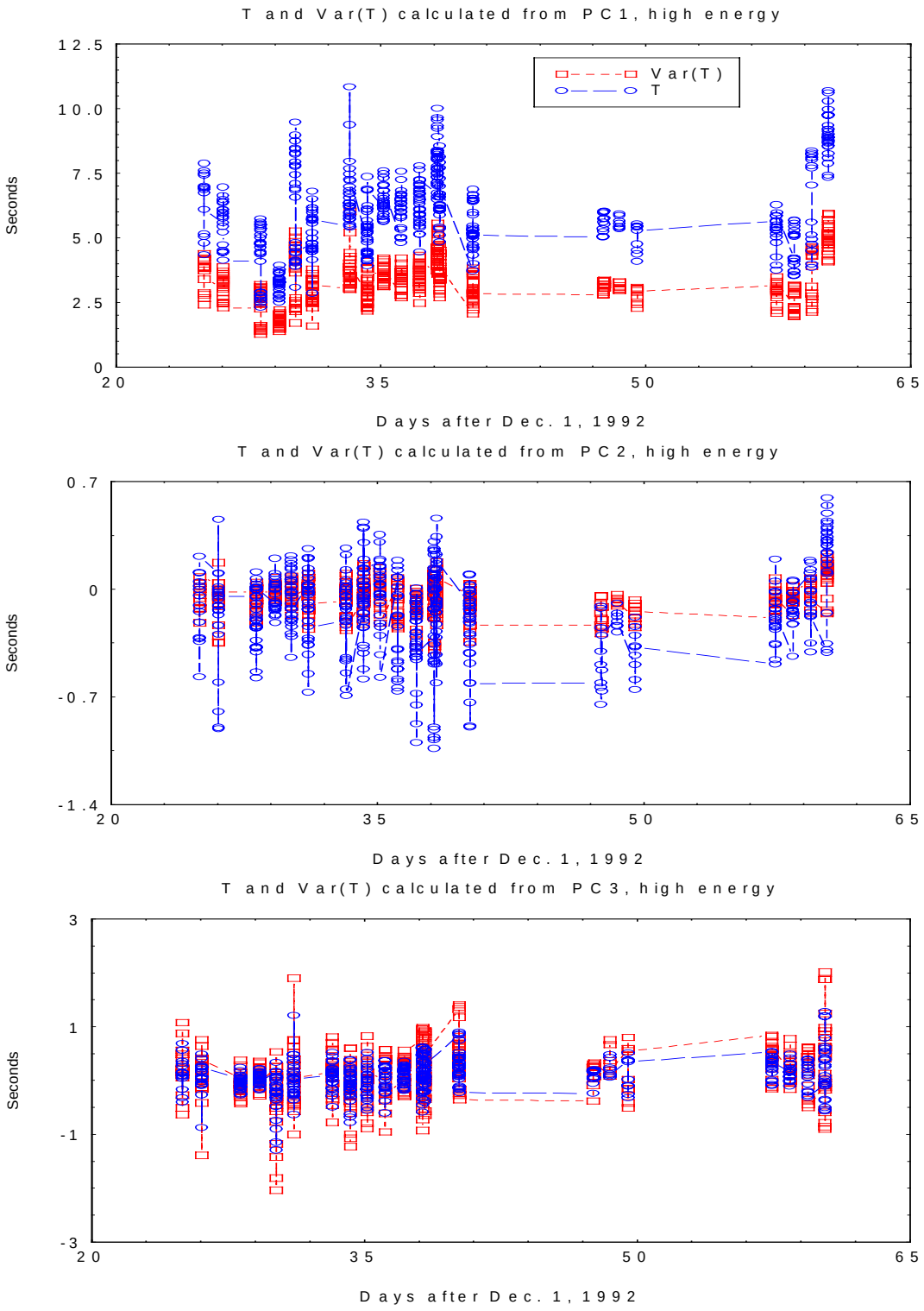

Fig. 19. . Temporal variations of the average time interval between 32 photons, T, and Var(T) averaged over all 4 areas, corresponding to the significant principal components: PC1, PC2 and PC3. File # 1273, high energy.

It may be of interest to study the fine structure of the temporal variations within single observing periods. An example for the file #1241 is shown in Fig. 20. The upper diagram corresponds to low energy, the lower diagram to high energy. The high energy plot shows again a rapid increase of the photon flux, while there is no

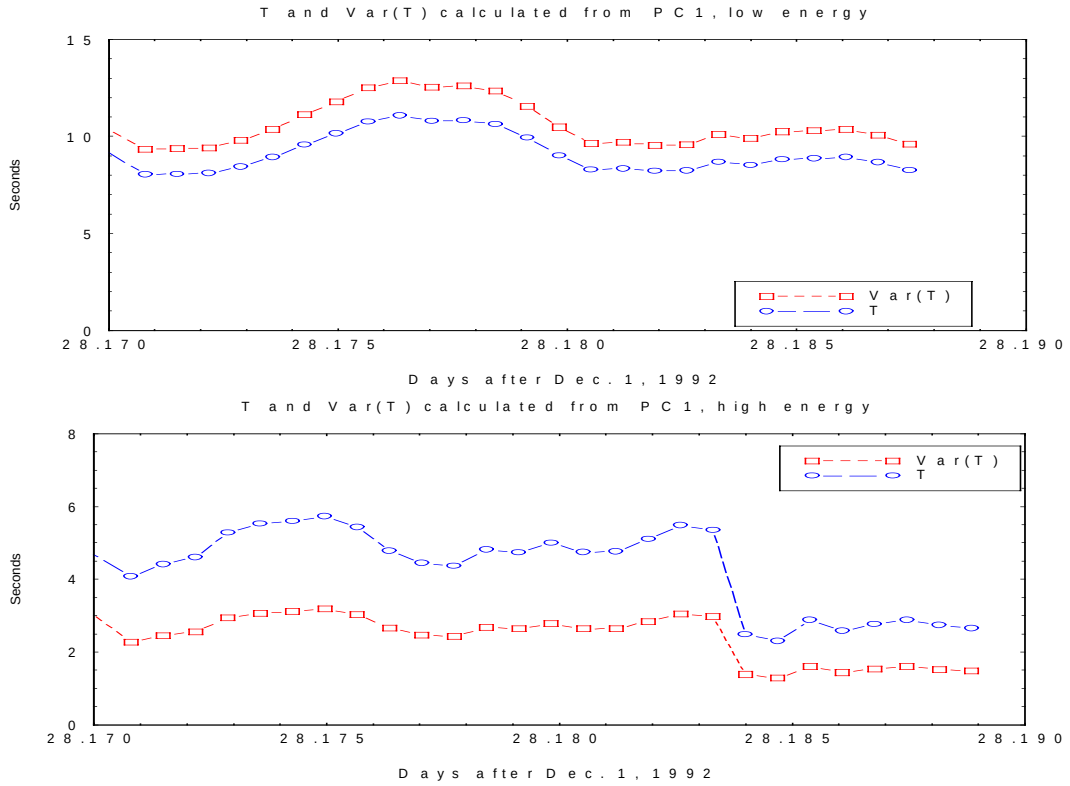

Fig. 20. Temporal variations, averaged over all 4 areas, within a single observing periods, (file #1241). The upper diagram corresponds to low energy, the lower diagram to high-energy photons.

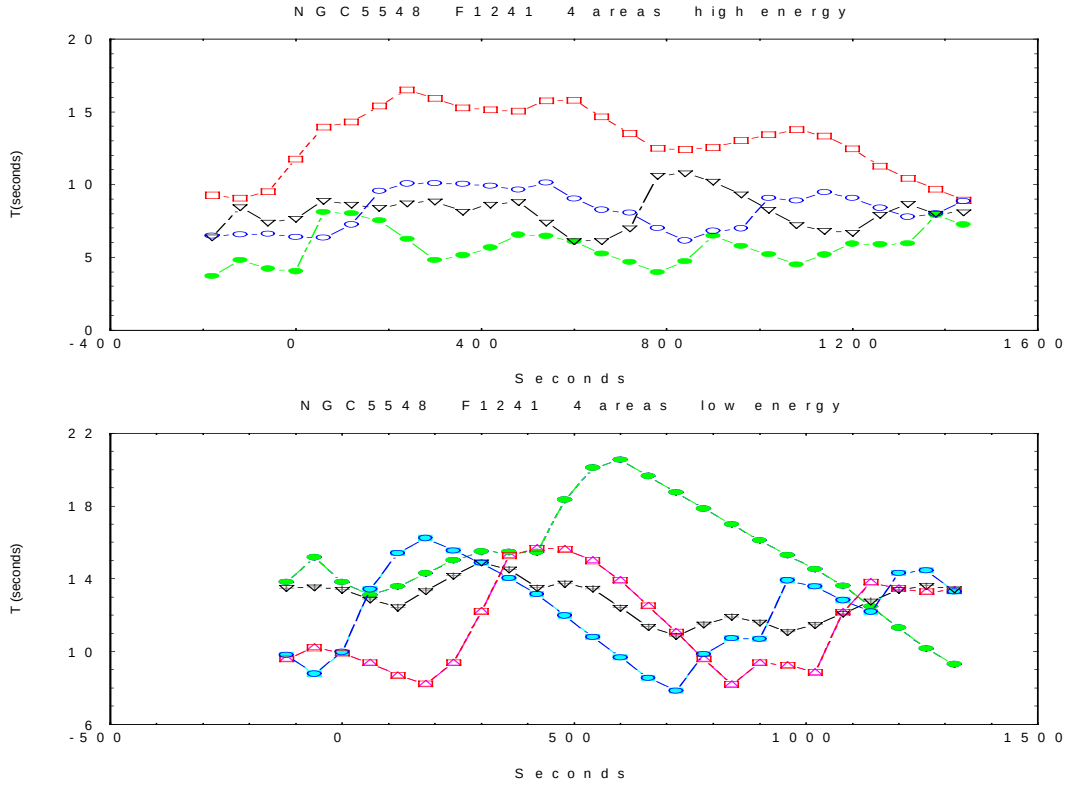

Fig. 21. The original values of T for all 4 areas and the file #1241, the same file as shown in resolved form in Fig. 20. Low energy photons are shown in the upper diagram, high-energy photons in the lower.

corresponding increase at low energy. Another interesting feature is that for the main component (may even be seen in Figs. 18 and 19) Var(T) has larger values than T at low energies. The opposite situation is observed at high energies.
The same case, as shown in Fig. 20, but not resolved into components, is shown in Fig. 21. Also data for all 4 areas are shown separately. It may be seen that it is extremely difficult to discover in Fig. 21 the time variations clearly visible in Fig 20.

It may be concluded, that the procedure of dividing the interesting part of the image into areas and than analyzing T and Var(T) by means of the principal component method may be very useful in searching for the true temporal variations in the photon data.

Temporal variations of photon counts

The above analysis may be repeated for photon counts. Instead of using the average time between 32 photons, photons were counted during a constant time interval. In order to perform the 4-area analysis, photons were counted during 20 seconds intervals in order to obtain large enough number of counts in each interval. The same image area, 30 x 30 pixels, as in the above study, was used. Photon counts normalized to the area of observation were used in the present study. Photon counts per second and a square pixel of the image core calculated for the entire sequence of 24 files and photon energy > 0.5 keV are shown in Fig.22.

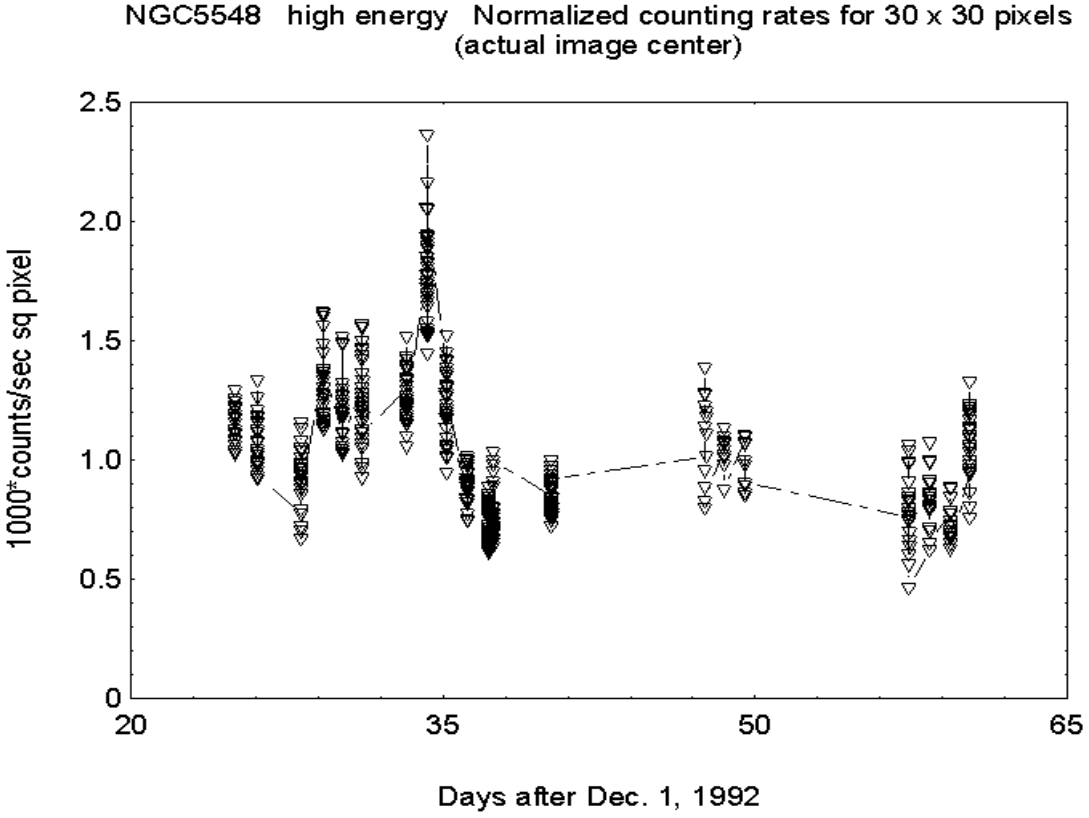

Fig. 22. Photon counts per second and a square pixel of the image core calculated for the entire sequence of 24 files. Photon energy > 0.5 keV.

Performing the principal component analysis using photon counts and their variances in all 4 areas it is possible to separate different components of photon counts, in the same way as it was done for the average time between photons.
Examples in Figs. 23 below show normalized observed counting rates together with normalized counting rates calculated from PC1, which is assumed to correspond the real temporal variation originated in the source.

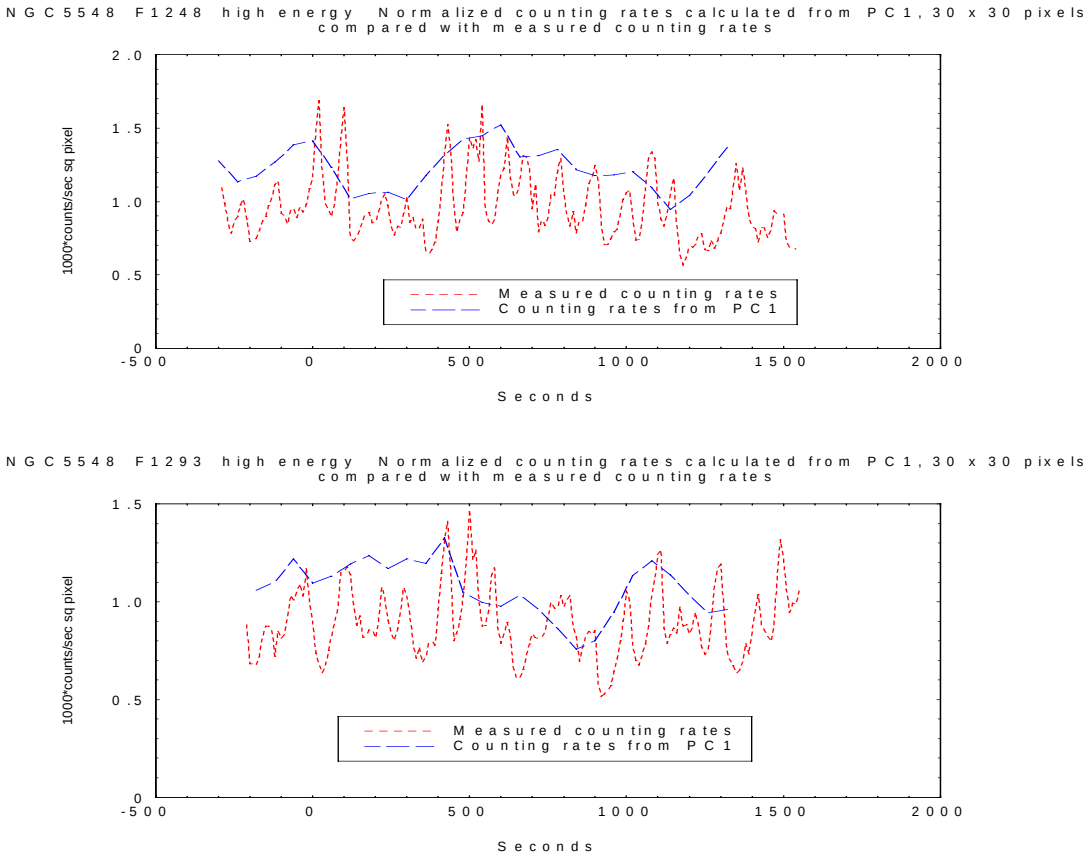

Fig. 23. Normalized counting rates calculated from PC1, 30 x 30 pixels, compared with measured counting rates . Source: NGC5548, files # 1248 and 1292, photon energy > 0.5 keV.

Conclusion

Multivariate statistical methods may be used to validate the structure of the X-ray image and to extract the true temporal variations of the photon flux.

Acknowledgement

The ROSAT data were accessed at the web address: ftp://heasarc.gsfc.nasa.gov. The directory /rosat/doc/archive contains listings of available data.

References

Glymour, C., Scheines, R., Spirtes, P. and Kelly, K.: Discovering Causal Structure - Artificial Intelligence, Philosophy of Science and Statistical Modelling, Academic Press 1987.

Morse, J. A., A. S. Wilson, M. Elvis and K.A. Weaver: Extended soft X-ray emission in Seyfert galaxies: ROSAT HRI observations of NGC3516, NGC4151 and Markarian 3. Astrophysical Journal, 439, p.121, 1995.
Spirtes, P., Scheines, R., Glymour, C. and Meek, C.: TETRAD II: Tools for Discovery (1993), Manuscript available from the Dept. of Philosophy, Carnegie Mellon University.

Appendix 1

ROSAT files used in the present study
X-ray source: NGC5548

wp701238n00
wp701239n00
wp701241n00
wp701242n00
wp701243n00
wp701244n00
wp701246n00
wp701247n00
wp701248n00
wp701249n00
wp701270n00
wp701271n00
wp701273n00
wp701275n00
wp701276n00
wp701277n00
wp701279n00
wp701280n00
wp701281n00
wp701282n00
wp701290n00
wp701291n00
wp701292n00
wp701293n00

Appendix 2

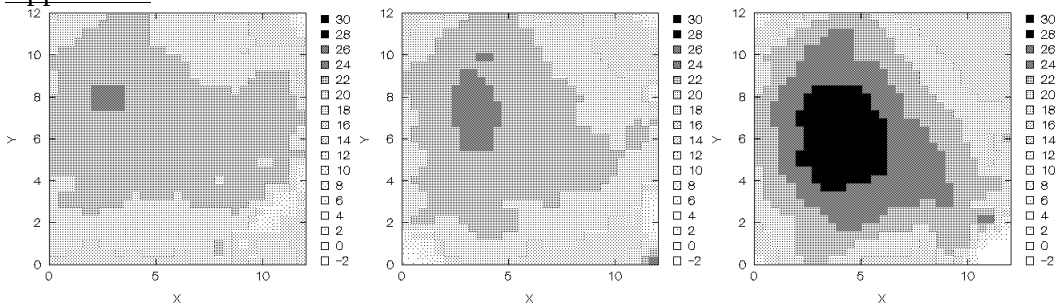

Dec. 24 Dec. 26 Dec. 28

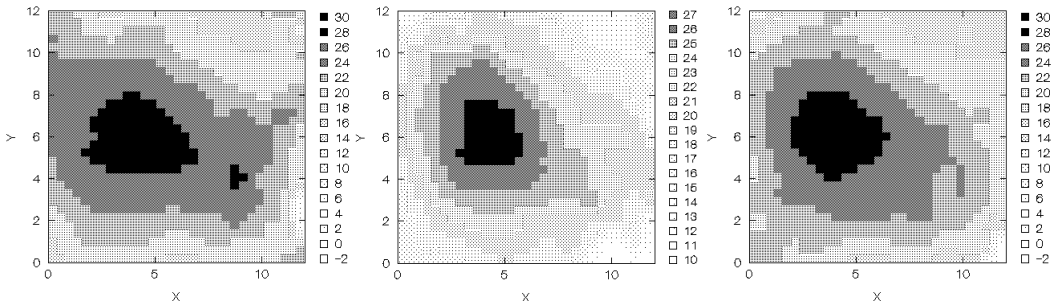

Dec. 29 Dec. 30 Dec. 31

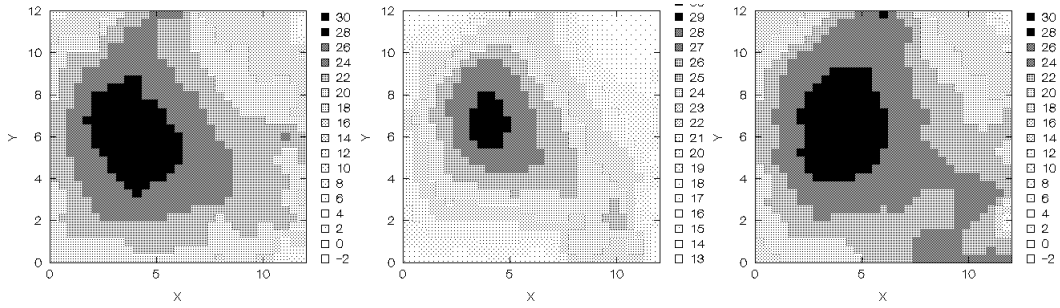

Jan. 2 Jan. 3 Jan. 4

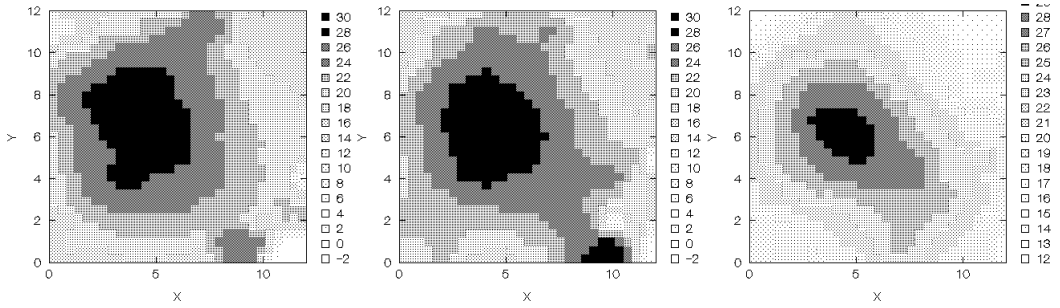

Jan. 5 Jan. 6 Jan. 6

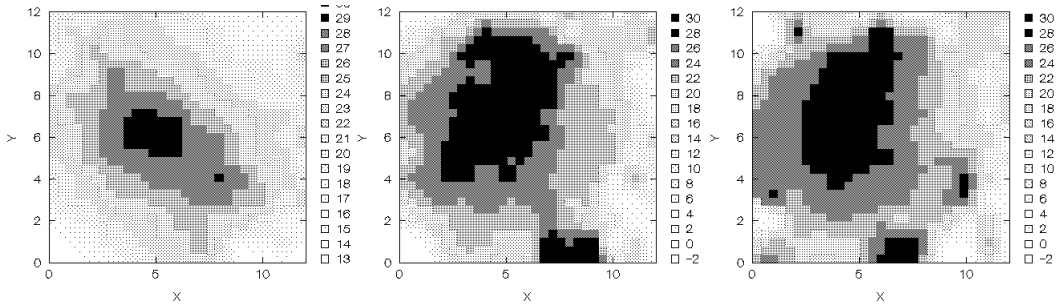

Jan. 9 Jan. 11 Jan. 15

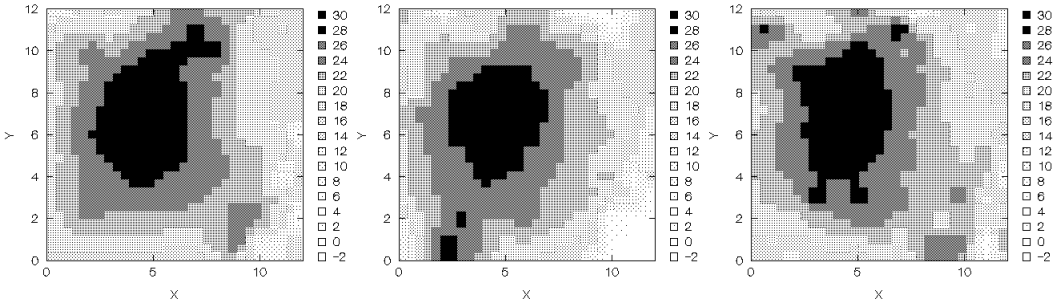

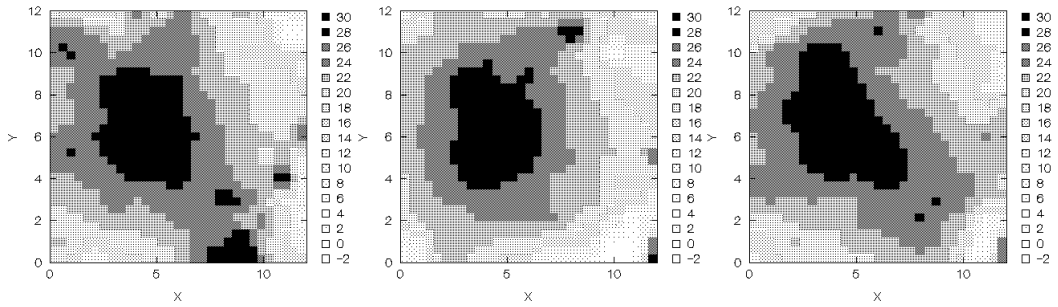

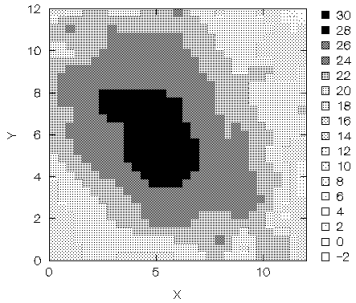

NGC 5548: Isoplots of average energy channel in the image, low energy part of the energy spectrum (PI < 52), December 1992 - January 1993.

Appendix 3.

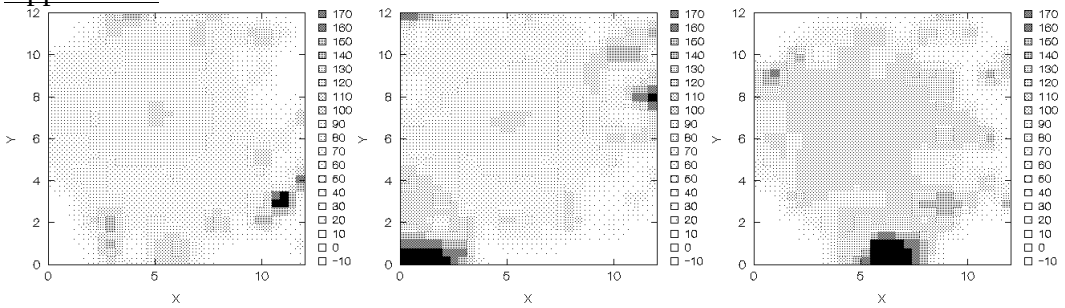

Dec. 24 Dec. 26 Dec. 28

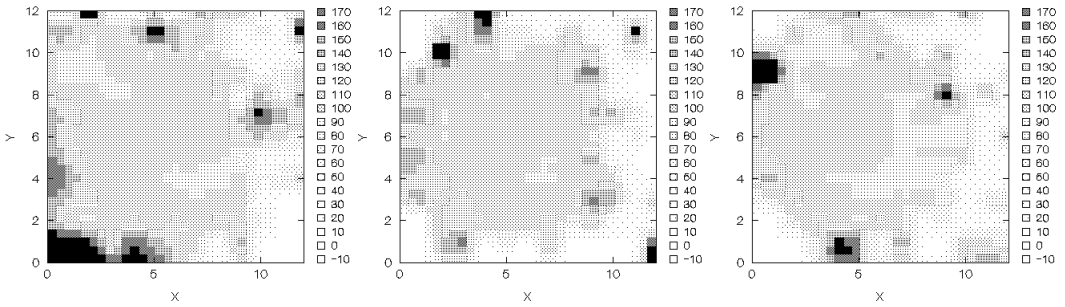

Dec. 29 Dec. 30 Dec. 31

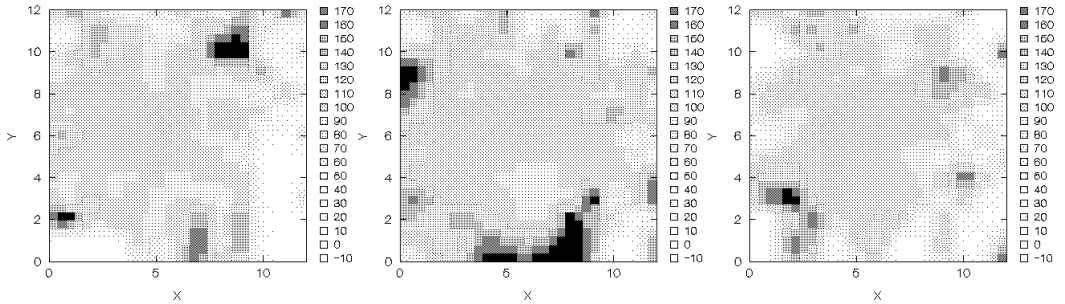

Jan. 2 Jan. 3 Jan. 4

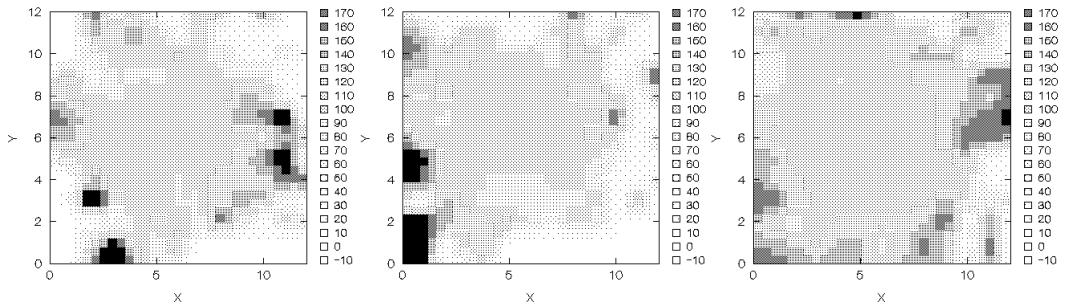

Jan. 5 Jan. 6 Jan. 6

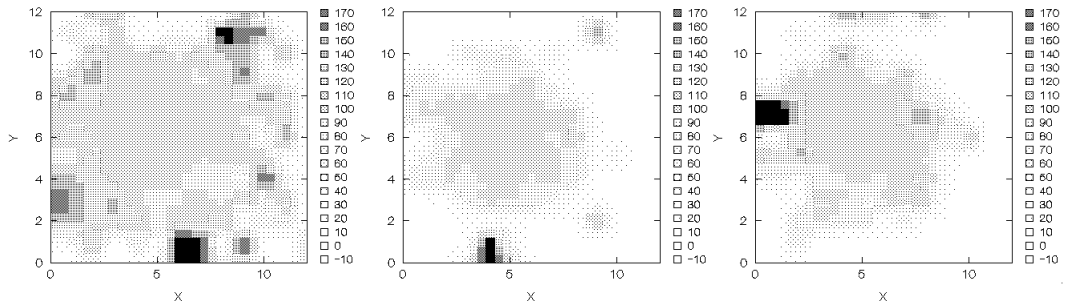

Jan. 9 Jan. 11 Jan. 15

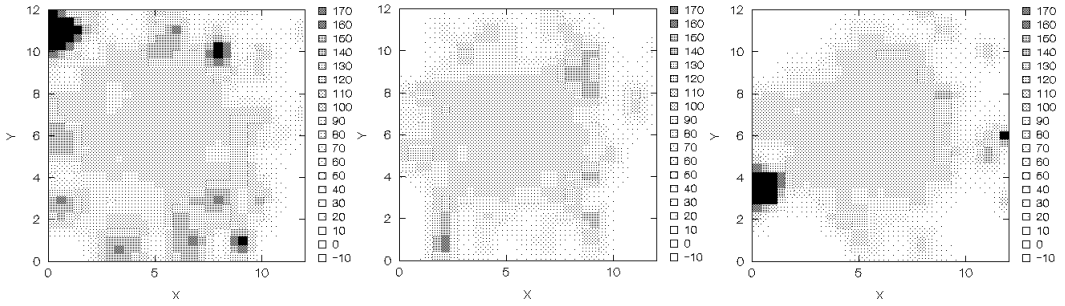

Jan. 16 Jan. 17 Jan 18

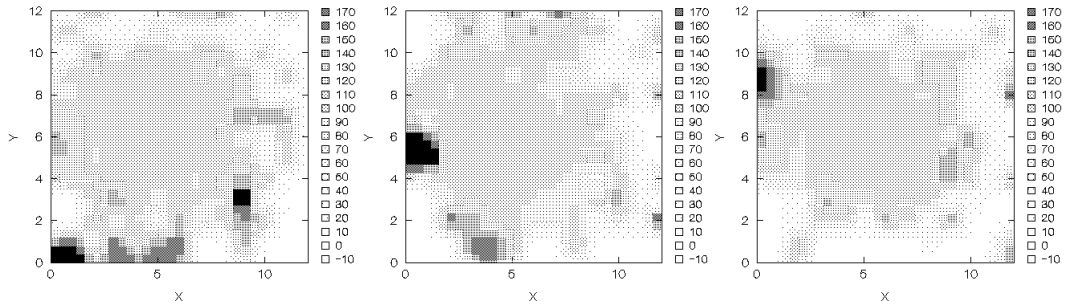

Jan. 26 Jan. 27 Jan. 28

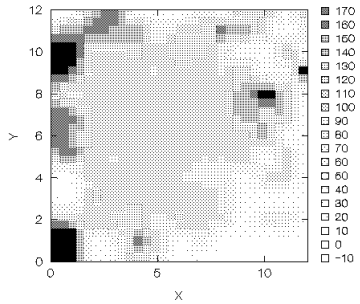

Jan. 29

NGC 5548: Isoplots of average energy channel in the image, high energy part of the energy spectrum (PI > 52), December 1992 - January 1993.

Appendix 4

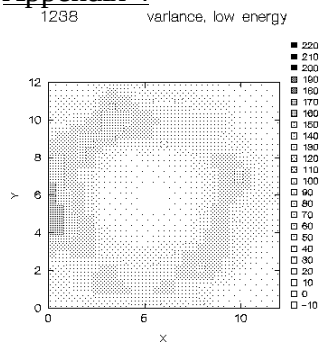

Dec. 24

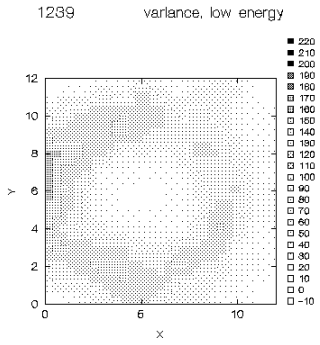

Dec. 26

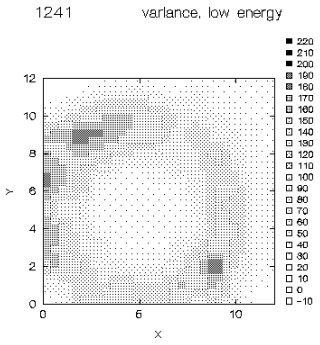

Dec. 28

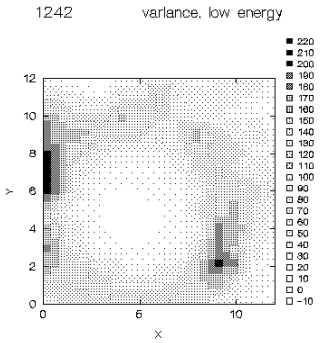

Dec. 29

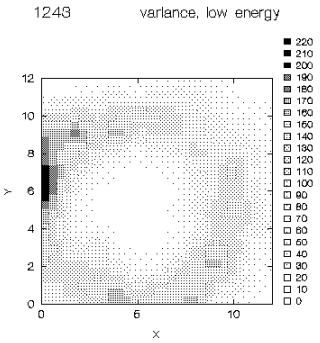

Dec. 30

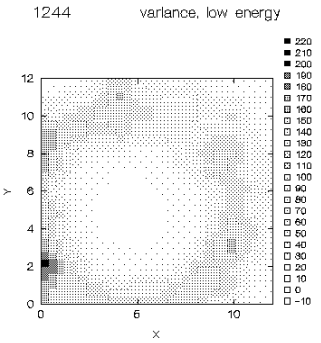

Dec. 31

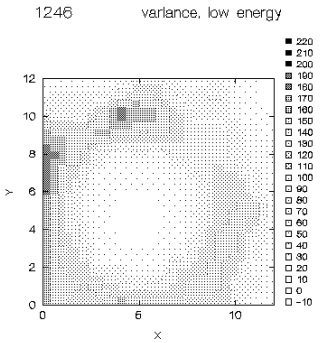

Jan. 2

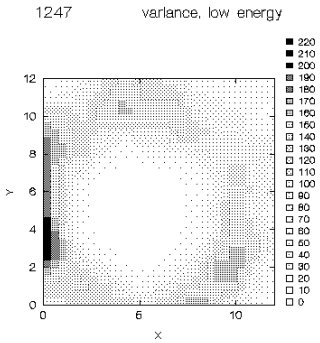

Jan. 3

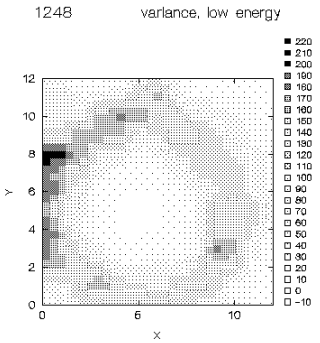

Jan. 4

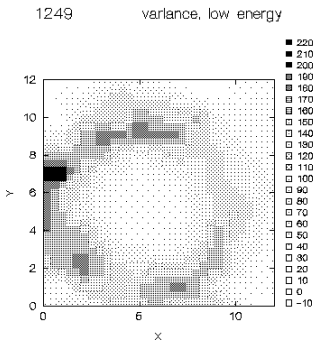

Jan. 5

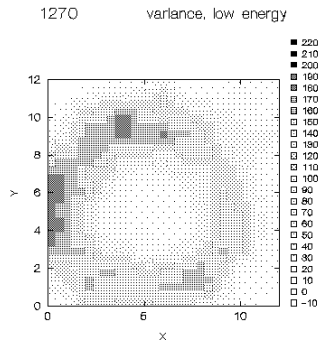

Jan. 6

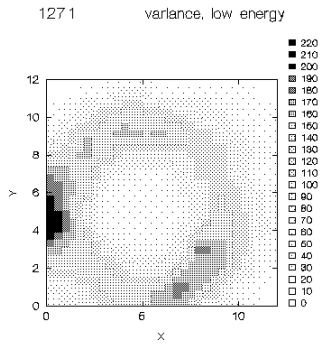

Jan. 6

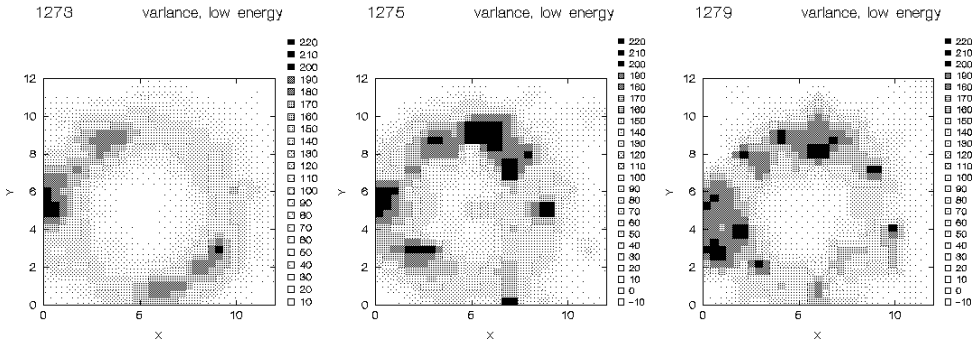

Jan. 9 Jan. 11 Jan. 15

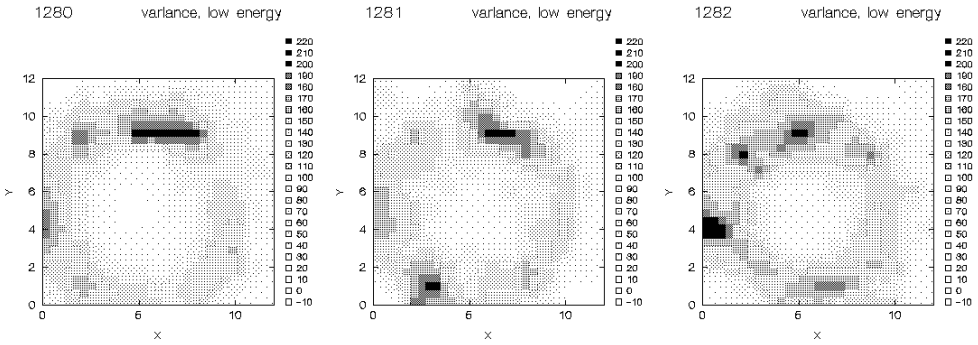

Jan. 16 Jan. 17 Jan. 18

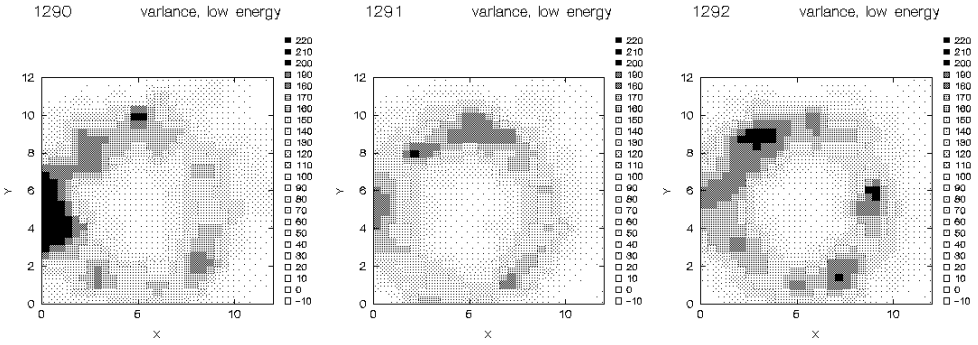

Jan. 26 Jan. 27 Jan. 28

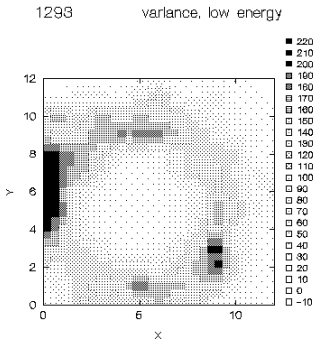

Jan. 29

NGC 5548: Isoplots of the energy variance in the image, low energy part of the energy spectrum (PI<52), December 1992 - January 1993.

Appendix 5

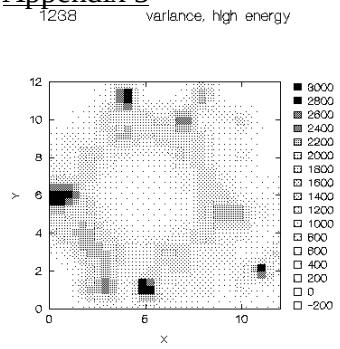

Dec. 24

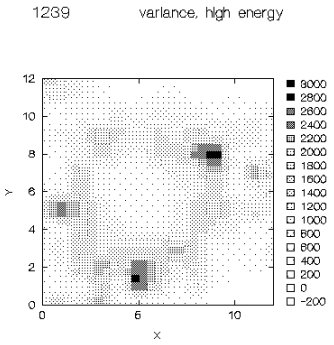

Dec. 26

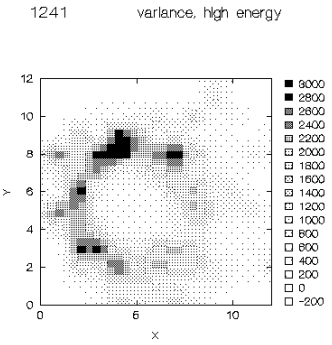

Dec. 28

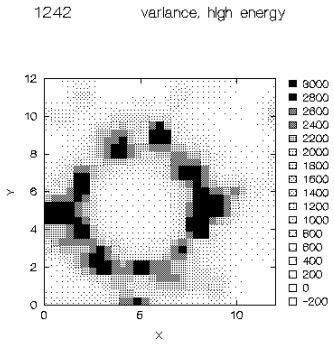

Dec. 29

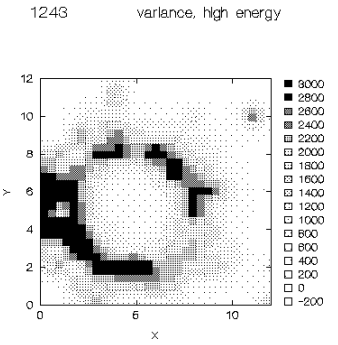

Dec. 30

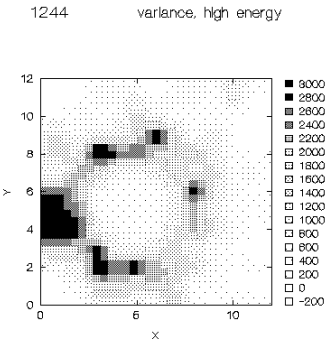

Dec. 31

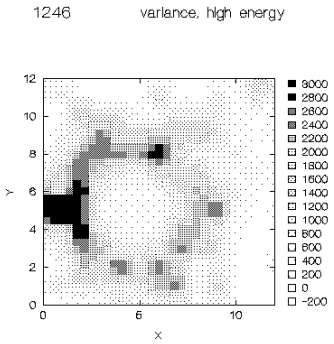

Jan. 2

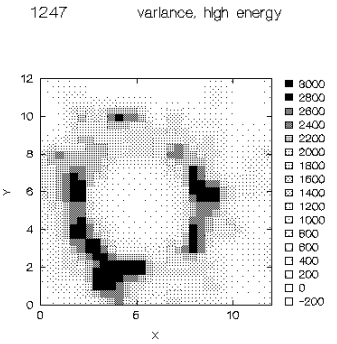

Jan. 3

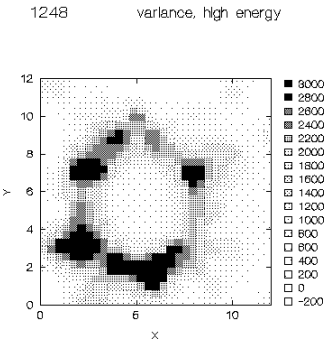

Jan. 4

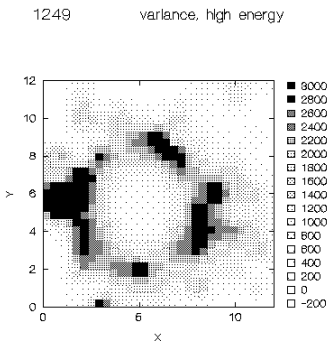

Jan. 5

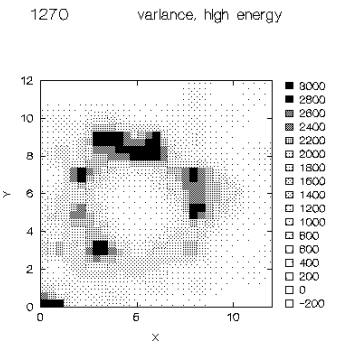

Jan. 6

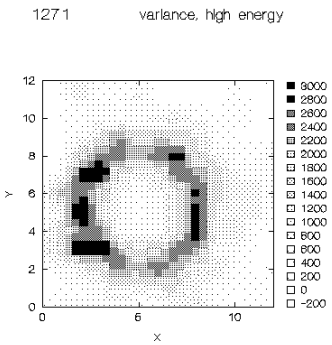

Jan. 6

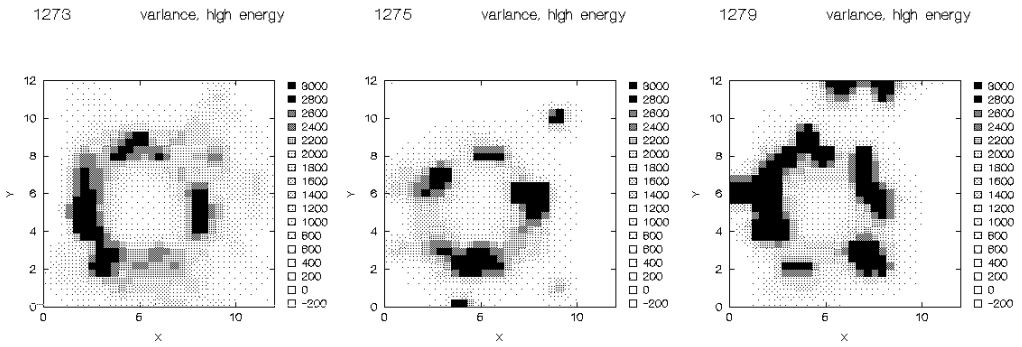

Jan. 9 Jan. 11 Jan. 15

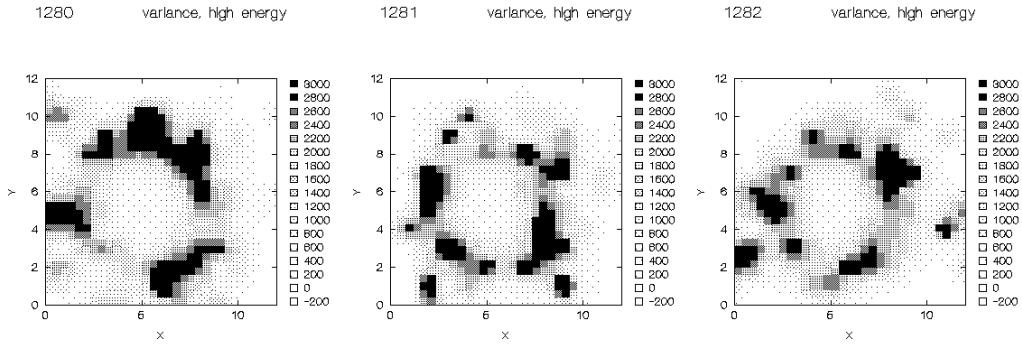

Jan. 16 Jan. 17 Jan. 18

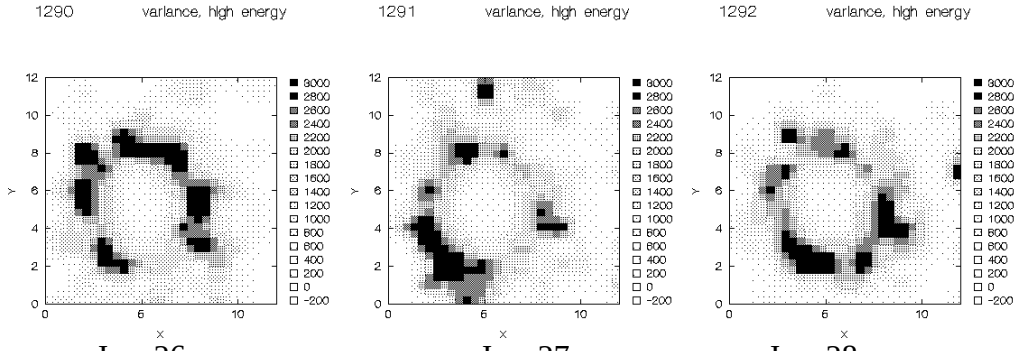

Jan. 26 Jan. 27 Jan. 28

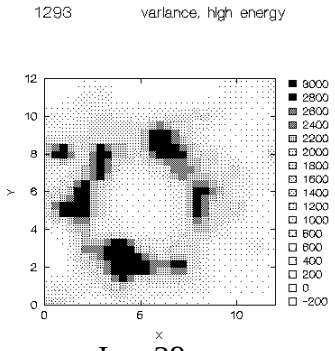

Jan. 29

NGC 5548: Isoplots of the energy variance in the image, high energy part of the energy spectrum (PI >52), December 1992 - January 1993.